JOURNAL
OF
PHYSICS OF THE EARTH

Volume III September 1955 Number 1

CONTENTS

PUBLISHED BY
THE SEISMOLOGICAL SOCIETY OF JAPAN

JOURNAL OF PHYSICS OF THE EARTH

The object of the publication of JOURNAL OF PHYSICS OF THE EARTH is to provide an international medium for the publication of original contributions in the field of geophysical science, more particularly concerning with physical properties and conditions of and phenomena occurring in the solid part of the earth.

The JOURNAL is open to any one who wishes to contribute his (or her) article. But the authors are, in principle, requested to pay page charges necessary for publishing their respective articles. The authors receive 100 copies of reprints free of charge.

In order to serve the purposes for which this JOURNAL is published, all contributions should be written in widely understandable languages, such as English, French and German, etc. Contributions should be sent to the Editor or to one of the Associate Editors.

For the time being, this JOURNAL will be issued at variable prices and at irregular intervals. The price of this issue is 200 yen inside Japan and $1.00 for foreign countries, the latter including postage.

Is The Layer C (413-1000 km) Inhomogeneous?

By

Haruo MIKI.

Abuyama Seismological Observatory, Faculty of Science, Kyoto University, Kyoto, Japan.

Abstract

There are opinions that the part of the earth's mantle is not homogeneous. $1-g^{-1}\frac{d\phi}{dr}$ which was first introduced by BULLEN (1949), the calculation of velocities of seimic waves (BIRCH, 1939) and the density distribution based on WILLIAMSON-ADAMS-BULLEN's method (BIRCH, 1954) have been thought as the evidences to show that these opinions are valid. The method developed in this paper shows that the density distribution can be derived without the assumption of hydrostatic equilibrium within the earth's mantle. The results obtained in the present paper show that the abnormal characters of the layer C (413–1000 km) can be explained by the non-hydrostatic equilibrium state of the layer instead of its inhomogeneity.

§ 1. We calculate the variation of GRÜNEISEN's ratio within the earth by considering the pressure effect on it alone, as the temperature effect on the GRÜNEISEN's ratio is known to be small. The experimental estimation of the pressure effect has not yet been performed and we can rely only on the theoretical one.

We can get the relationship between γ_G and V if the relation between ν_m and V or v and V are known, for the definition of the GRÜNEISEN's ratio is as follows:

$$\gamma_G=-\frac{\partial \log \nu_m}{\partial \log V} \tag{1}$$

where

$$\nu_m=\left(\frac{9}{4\pi}\frac{N}{V}\frac{1}{\frac{1}{v_p{}^3}+\frac{2}{v_s{}^3}}\right)^{\frac{1}{3}}, \tag{2}$$

V: molar volume,

N: LOSCHMIDT's number,

v_p, v_s: velocities of longitudinal and transversal elastic waves, respectively,

ν_m: DEBYE's maximum frequency,

ν_G: GRÜNEISEN's ratio.

BIRCH (1939) has shown that

$$\frac{V_o}{V}=(1+2f)^{3/2} \tag{3}$$

$$v_p{}^2=v_{po}{}^2(1+2f)\left(1+f\frac{11m+10}{m+2}\right) \tag{4}$$

$$v_s{}^2=v_{so}{}^2(1+2f)\{1+f(3m+4)\} \tag{5}$$

where f: negative strain,

$$m=\frac{v_{po}{}^2}{v_{so}{}^2}-2\,,$$

V_o, v_{po}, v_{so}: molar volume, velocities of longitudinal and transversal waves at zero pressure, respectively.

We can obtain the following expression for γ_G by inserting the above equations into (1) and (2).

$$\gamma_G=\frac{1}{3}+\frac{1}{3}\frac{1}{v_{so}{}^3\sqrt{\{1+f(3m+4)\}^3}+2v_{po}{}^3\sqrt{\left(1+f\frac{11m+10}{m+2}\right)^3}}$$
$$\times\left\{v_{so}{}^3\sqrt{\{(1+f(3m+4)\}^3}\ \frac{\frac{1}{2}\frac{13m+4}{m+2}+2f\frac{11m+10}{m+2}}{1+f\frac{11m+10}{m+2}}\right.$$
$$\left.+\,v_{po}{}^3\sqrt{\left(1+f\frac{11m+10}{m+2}\right)^3}\frac{3m+6+4f(3m+4)}{1+f(3m+4)}\right\} \tag{6}$$

On the other hand, BIRCH (1952) has obtained the approximate expression for γ_G as follows. Using the expression of ν_m in terms of adiabatic bulk modulus K_s, density ρ and POISSON's ratio σ

$$\nu_m = \text{const.}\left(\frac{K_s}{\rho^{1/3}}\right)^{1/2} F(\sigma) \tag{7}$$

and the following formula for γ_G

$$\gamma_G = \frac{\partial \log \nu_m}{\partial \log \rho} \tag{8}$$

we can obtain the following equation

$$\gamma_G = -\frac{1}{6} + \frac{1}{2}\left(\frac{\partial K_T}{\partial P}\right)_T \tag{9}$$

provided that the effect of $F(\sigma)$ on γ_G is neglible and the equality $\partial \log K_s/\partial \log \rho = (\partial K_T/\partial P)_T$ is assumed. Rewriting the second term of the right-hand-side of (9) by means of the theory of finite strain, we get the expression for γ_G as the function of f as follows:

$$\gamma_G = -\frac{1}{6} + \frac{1}{2}\,\frac{12+49f}{3(1+7f)} \tag{10}$$

We have obtained the above two relationships between γ_G and f but both methods have their good points and bad points. Thus, in order to obtain γ_G by means of (6), we must know the velocities of elastic waves at zero pressure, but we have no method of estimating these values without knowing the material composing the earth's interior. On the other hand, γ_G as the function of f can be obtained immediately by using (10) but some errors are expected in the estimation, because in getting (10), we have made several neglects and assumptions. Both methods have also some errors resulted from the fact that the theory of finite strain is not so complete at present. Furthermore, elastic constants concerning the velocities of elastic waves are the adiabatic ones but in deriving (4) and (5), we use the isothermal ones.

Fig. 1. shows the relationships between γ_G and f by means of (10) and (6) for various combinations of v_{p0} and v_{s0}. The combinations adopted are as follows:

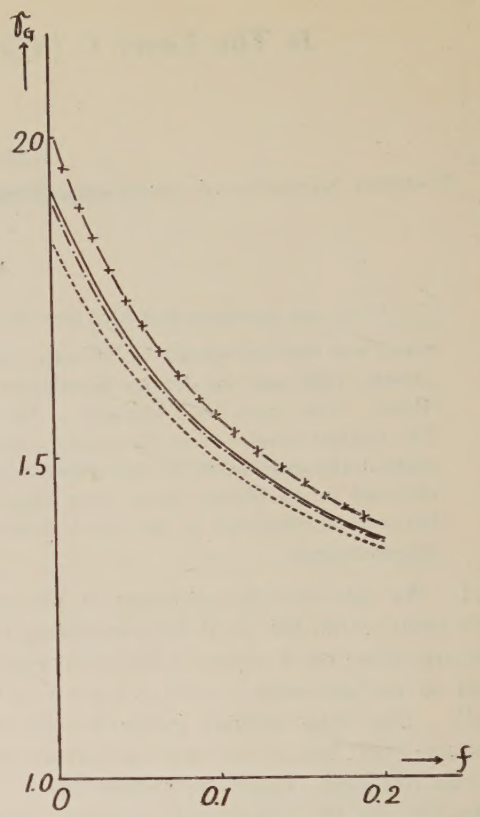

Fig. 1. Diagrams of GRÜNEISEN's ratio versus negative strain.
——— $v_{p0}=7.75$ km/sec, $v_{s0}=4.35$ km/sec.
—·—·— $v_{p0}=7.60$ km/sec, $v_{s0}=4.30$ km/sec.
—×—×— $v_{p0}=8.75$ km/sec, $v_{s0}=4.77$ km/sec.
- - - - - - - by means of (10).

(1) $v_{p0}=7.75$ km/sec, $v_{s0}=4.35$ km/sec,
(2) $v_{p0}=7.60$ km/sec, $v_{s0}=4.30$ km/sec,
(3) $v_{p0}=8.75$ km/sec, $v_{s0}=4.77$ km/sec,
(4) by means of (10).

We see from Fig. 1 that the GRÜNEISEN's ratio derived from (10) and (6) on various combinations of v_{p0} and v_{s0} decreases with increasing negative strain in nearly the same manner.

§ 2. In order to obtain the relationships between the depths and GRÜNEISEN's ratios or negative strains, we divide the earth's mantle into many thin spherical shells. We assume

(1) Seismic velocities at the depth of 33 km after BULLEN (1947).

(2) (3) Seismic velocities adopted by BIRCH (1939) at zero pressure for the region shallower than the depth of 600 km and deeper than the depth of 700 km, respectively.

$f=0.000$ at the surface of the earth mantle which is at the depth of 33 km, and put the inner boundary of the first spherical shell at the depth where $f=0.005$. We assume in this spherical shell that the composition and structure of material does not change and GRÜNEISEN's hypothesis (SLATER, 1939)

$$\nu=\frac{\text{const.}}{V^{\gamma_G}} \tag{11}$$

holds, then we can obtain the following equation

$$\left(\frac{V_1}{V_2}\right)^{3\gamma_G-1}=\frac{\left(\frac{1}{v_p{}^3}+\frac{2}{v_s{}^3}\right)_1}{\left(\frac{1}{v_p{}^3}+\frac{2}{v_s{}^3}\right)_2} \tag{12}$$

by inserting (2) into (11). On that occasion, we put the DEBYE's maximum frequency ν_m equal to the lattice frequency ν (UFFEN, 1952). Suffixes 1 and 2 denote the physical quantities at the inner and outer surface of the spherical shell. The left-hand-side of (12) can be estimated as the value of f at the outer and inner surfaces of the spherical shell and the mean value of γ_G are the known quantities. The denominator of the right-hand-side of (12), $(v_p{}^{-3}+2v_s{}^{-3})_2$, is the value at the outer surface of the first shell, i.e., at the depth of 33 km, and can be estimated from the observed seismic velocities. Thus, we can get the value of $(v_p{}^{-3}+2v_s{}^{-3})_1$ in (12). We can estimate the depth of inner surface of the first spherical shell provided that we have the relationship between the depth and $(v_p{}^{-3}+2v_s{}^{-3})$ beforehand (Fig. 2). Seismic velocities necessary in the calculation are adopted from BULLEN's book (1947).

The second spherical shell is formed as follows. We may consider the strain at the outer surface of the second spherical shell is equal to the one at the inner surface of the first spherical shell, $f=0.005$, since the strain of the material is continuous within the earth's mantle. We put the inner surface of the second spherical shell at the depth where $f=0.015$. The value of $(v_p{}^{-3}+2v_s{}^{-3})_2$ at the outer surface of the second spherical shell is known from Fig. 2. The mean value of γ_G in this shell can be known from Fig. 1 and the value

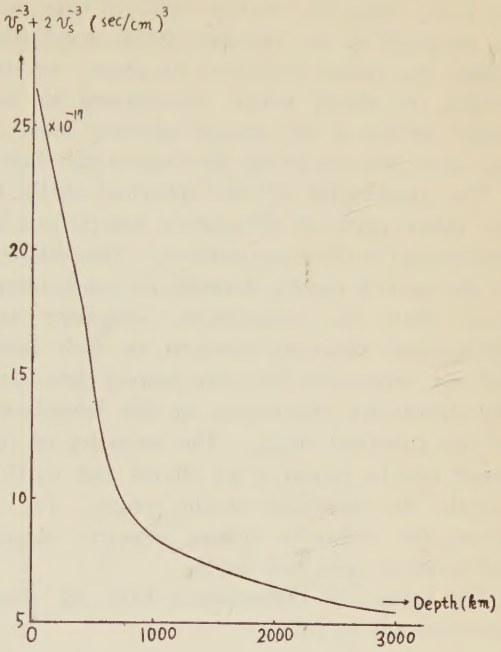

Fig. 2. Diagram of $v_p{}^{-3}+2v_s{}^{-3}$ versus cepth.

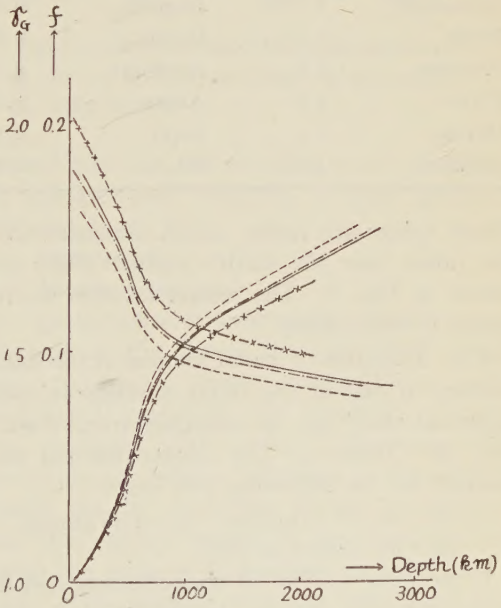

Fig. 3. Diagrams of depth versus γ_G and negative strain.

——— $v_{po}=7.75$ km/sec, $v_{so}=4.35$ km/sec.
—·—·— $v_{po}=7.60$ km/sec, $v_{so}=4.30$ km/sec.
—×—×— $v_{po}=8.75$ km/sec, $v_{so}=4.77$ km/sec.
– – – – – – by means of (10).

of V_1/V_2 from (3), for the strain in this shell is assumed to be between 0.005 and 0.015. Using the values estimated as above, we can obtain the depth which corresponds to the inner surface of the second spherical shell in the same way as in the first spherical shell.

The boundaries of the spherical shells in the other parts of the earth's mantle can be determined in the same manner. This division of the earth's mantle depends on the assumptions that the composition, structure and GRÜNEISEN's ratio are constant in each shell, but not necessarily the same among them, and the strains are continuous at the boundaries of the spherical shells. The accuracy of the result can be raised if we divide the earth's mantle into narrower strain ranges. Fig. 3 shows the relations among negative strain, GRÜNEISEN's ratio and depth.

The values of GRÜNEISEN's ratio of some minerals are as follows:

Table 1. GRUNEISEN's ratios of minerals

Corundum	1.7	Diopside	0.8
Rutile	1.7	Quartz	0.8
Periclase	1.6	Anorthite	0.7
Pyrite	1.6	Albite	0.5
Olivine	1.2	Beryl	0.4
Diamond	1.0	Zircon	0.4

These values are rather small, compared with the values near the earth's surface which are shown in Fig. 3. The reason for this discrepancy is not known.

§ 3. The ratio of molar volume at the inner surface to that at the outer surface of each spherical shell can be obtained from Fig. 3 and (3). (Table 2) The calculations are performed for the following two cases

(1) $v_{po}=7.75$ km/sec, $v_{so}=4.35$ km/sec.
(4) by means of (10).

If we assume that no discontinuous density change occurs at the boundaries of each spherical shell by the change of composition, the lattice structure and etc., the density distribution, mass and moment of inertia of the earth's mantle can be estimated, taking the density at the depth of 33 km ρ_{33} as a parameter. The results of calculations are as follows:

Table 2. The ratio of molar volume at the inner surface to that at the outer surface of each spherical shell.

Shell number	V_1/V_2	Depth (km) (1)	Depth (km) (4)
		33	33
1	0.9852	102	98
2	0.9710	235	226
3	0.9716	355	340
4	0.9721	443	432
5	0.9726	502	489
6	0.9731	552	539
7	0.9736	595	582
8	0.9740	678	647
9	0.9745	758	726
10	0.9749	872	797
11	0.9753	1050	952
12	0.9757	1330	1171
13	0.9761	1656	1460
14	0.9765	2013	1789
15	0.9769	2389	2145
16	0.9772	2790	2505
17	0.9775	2898	2898

(1) $M_m=1.1469\rho_{33}\times10^{27}$ gr,
$I_m=2.0244\rho_{33}\times10^{44}$ gr.cm^2.
(2) $M_m=1.1591\rho_{33}\times10^{27}$ gr,
$I_m=2.0473\rho_{33}\times10^{44}$ gr.cm^2.

The mass and the moment of inertia of the earth's core can be obtained, taking the central density ρ_c as a parameter provided that the density distribution in the earth's core can be obtained by the WILLIAMSON and ADAMS method. Thus, the mass and the moment of inertia of the earth can be expressed by using two parameters ρ_{33}, ρ_c. These parameters can be settled by the observed values for the mass and moment of inertia of the earth. The results of the calculation are as follows:

(1) $\rho_{33}=3.46$ gr/cm^3 $\rho_c=12.41$ gr/cm^3
(4) $\rho_{33}=3.42$ gr/cm^3 $\rho_c=12.44$ gr/cm^3

By using the above values and the results in Table 2, we get the density distribution within the earth as shown in Fig. 4.

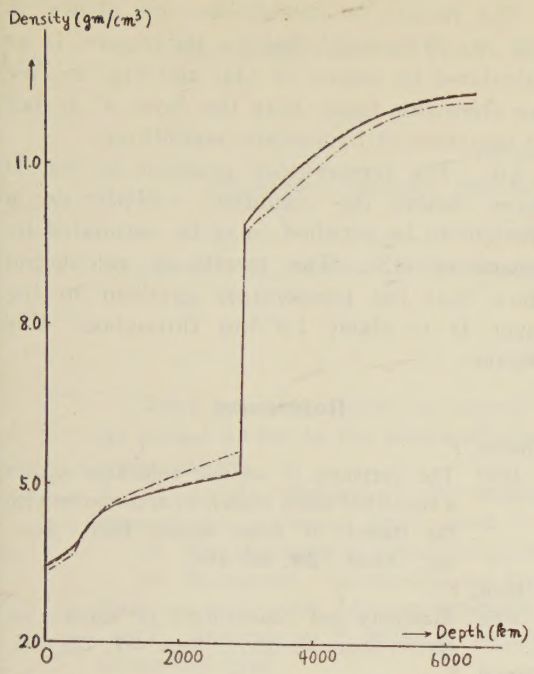

Fig. 4. Density distributions within the earth.
———— $v_{p0}=7.75$ km/sec, $v_{s0}=4.35$ km/sec.
- - - - - - - - by means of (10)
—·—·— after BULLEN.

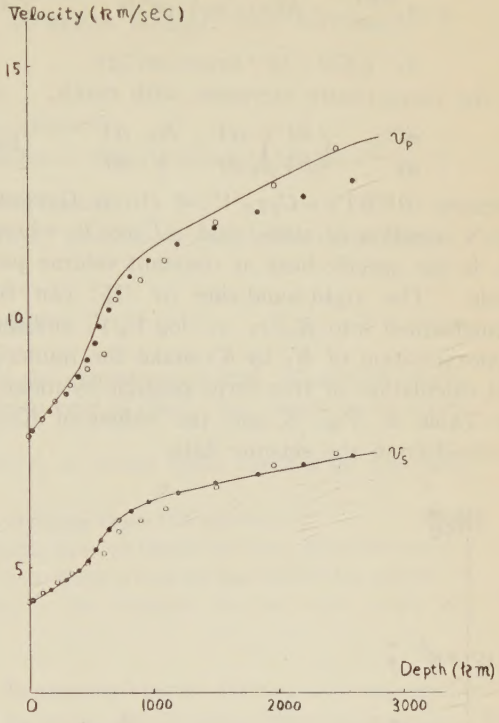

Fig. 5. Distributions of seismic velocities.
● by the method described in this paper.
○ after BIRCH.

BIRCH (1954) has shown that the initial density at the top of the mantle must be greater than 3.7~3.8 gr/cm³ in order to obtain the reasonable values for the mass and the moment of inertia of the core. But his method of calculation, i.e., WILLIAMSON-ADAMS-BULLEN's method, is based on the assumption that the earth's mantle is

isothermal,
homogeneous and
in the state of hydrostatic equilibrium.

This high value of the initial density, he thought, is one of the evidences that the layer C is not homogeneous. The calculation in this section, however, shows that the reasonable density distribution can be obtained from the assumption of homogeneity of the mantle.

§ 4. The distributions of the seismic wave velocities can be obtained by means of (4), (5) and Fig. 3. (Fig. 5) The solid lines in the figure show the observed values. The small circles after BIRCH (1939) are obtained under the assumption that the earth's mantle is divided into two layers which have the different seismic wave velocities at zero pressure and each layer is

isothermal,
homogeneous and
in the state of hydrostatic equilibrium.

We see in the figure that the black points calculated by the present method is a fairly good approximation to the variations of seismic velocities with depth. Therefore, the variations of seismic velocities in the earth's mantle can be explained by the assumption that the earth's mantle is homogeneous but not in the state of hydrostatic equilibrium.

§ 5. The pressure variation with depth is

$$\frac{dP}{dr}=\left(\frac{\partial P}{\partial V}\right)_T\frac{dV}{dr}+\left(\frac{\partial P}{\partial T}\right)_V\frac{dT}{dr} \qquad (13)$$

and equals to $-g\rho$ if the condition of hydrostatic equilibrium is satisfied within the earth, where

$$g=G\frac{M(r)}{r^2}\ ,\quad M(r)=4\pi\int_0^r \rho r^2 dr\ , \tag{14}$$

G: 6.670×10^{-8} dynes.cm^2/gr.

If the temperature increases with depth,

$$-\frac{dP}{dr}>-\left(\frac{\partial P}{\partial V}\right)_T\frac{dV}{dr}=\frac{K_T}{V}\frac{dV}{dr} \tag{15}$$

because $(\partial P/\partial T)_V=C_V\gamma_G/V>0$ (from GRÜNEISEN's equation of state) and $dT/dr<0$, where C_V is the specific heat at constant volume per mole. The right-hand-side of (15) can be transformed into $K_T/(r_2-r_1)\cdot\log V_2/V_1$ and the approximation of K_T by K_S make the numerical calculation of this term possible by means of Table 2, Fig. 3 and the values of K_S/ρ derived from the seismic data.

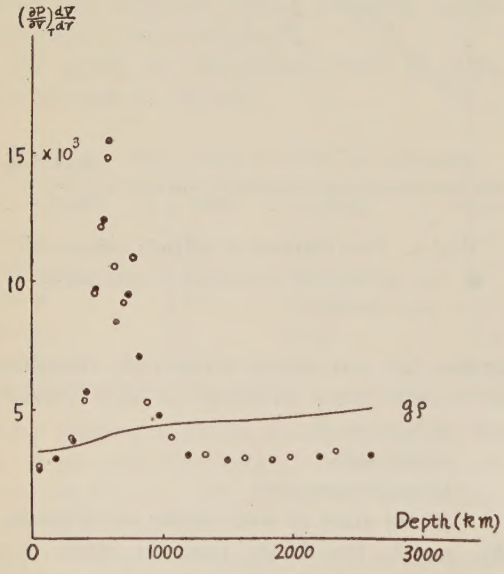

Fig. 6. Distributions of pressure gradient, neglecting the temperature effect.
● $v_{p0}=7.75$ km/sec, $v_{s0}=4.35$ km/sec.
○ by means of (10).

The results of calculations are shown in Fig. 6. The solid line in the figure is $g\rho$ calculated by means of (14) and Fig. 3. We see from this figure that the layer C is not in the state of hydrostatic equilibrium.

§ 6. The temperature gradient in the D layer, where the condition $-dP/dr=g\rho$ is thought to be satisfied, may be estimated by means of (13). The results of calculation show that the temperature gradient in the layer D is about 1.8°/km throughout this region.

References

BIRCH, F.:
1939 The variation of seismic velocities within a simplified earth model, in accordance with the theory of finite strain, Bull. Seis. Soc. Amer., **29**, 463–479.

BIRCH, F.:
1952 Elasticity and constitution of earth's interior, Jour. Geophys. Res., **57**, 227–286.

BIRCH, F.:
1954 Elasticity and constitution, Trans. Amer. Geophys. Union, **35**, 79–85.

BULLEN, K. E.:
1947 "An introduction to the theory of seismology.", Cambridge, The Univ. Press.

MIKI, H.:
1952 Three types of the distributions of temperature and density in the interior of the earth, Jour. Phys. Earth, **1**, 21–23.

MIKI, H.:
1954 Temperature distributions within the earth, Jour. Phys. Earth, **2**, 1–3.

SLATER, J. C.:
1939 "Introduction to chemical physics.", New York, McGraw-Hill Book Co.

UFFEN, R. J.:
1952 A method of estimating the melting point in the earth's mantle, Trans. Amer. Geophys. Union, **33**, 893–896.

Wave Generations from Line Sources within the Ground.

By
Hitoshi TAKEUCHI
Geophysical Institute, Faculty of Science, Tokyo University, Tokyo.
and Naota KOBAYASHI.
Department of Precision Mechanics, Faculty of Technology, Chūō University, Tokyo.

Abstract

Wave generations from line sources within the ground are studied. Numerical details are worked out for the line source of step function type in time. The results to be noted are as follows;

(1) At the "epicenter", the displacement is a simple pulse followed by a gradual decrease to a permanent displacement.

(2) RAYLEIGH waves appear at a certain distance from the epicenter.

(3) Permanent displacements are rather large even at points far away from the origin. They are comparable with the amplitudes of RAYLEIGH waves at the respective points.

(4) There is no S phase in seismograms to be obtained for the wave origin of dilatational type.

§ 1. The propagation of tremors over the surface of a semi-infinite elastic solid due to a line source at a certain depth below the free surface was discussed by H. LAMB (1904), H. NAKANO (1925) and E. R. LAPWOOD (1949). These authors were interested in the displacements at points far away from the wave origin, and did not study the tremors near the origin. Furthermore, by using the method of contour integral, they got some expressions for the displacements corresponding to the P, S and RAYLEIGH waves. As is understood easily, each component wave above cited has its duration time. Thus, in order to get the displacement at any time, we must sum up the contribution from each wave. In the course of this summing up process, some of the above waves may be masked by some other waves. In any of the above papers, this summing up process has not been made. Thus, in a strict sense, we do not know the exact time variations of the displacements even at points far away from the wave origin. In short, it is required in this kind of problem to get simple expressions by which the displacements at any point and at any time may easily be calculated. In the analysis to follow, such expressions will be given, and by using these expressions, some numerical examples will be worked out in detail.

§ 2. It was shown by NAKANO that for the compressional line source

$$u_0=\frac{\partial\phi}{\partial x}\,,\quad v_0=\frac{\partial\phi}{\partial y}\,,$$

$$\phi=\frac{\pi i}{2}e^{ipt}H_0^{(2)}(hR)$$

$$=-\int_0^\infty e^{i(pt-hR\cosh\phi)}d\phi\,,$$

where $R^2=x^2+(y-f)^2$,

$$h=p\sqrt{\frac{\rho}{\lambda+2\mu}}=\frac{p}{V_p} \tag{2.1}$$

at a depth f below the free surface, we have

$$u(x,\,y=0,\,t)=2ik^2\int_{-\infty}^{\infty}\frac{\beta\xi}{F(\xi)}e^{ipt+i\xi x-\alpha f}\,d\xi,$$

$$v(x,\,y=0,\,t)=k^2\int_{-\infty}^{\infty}\frac{2\xi^2-k^2}{F(\xi)}e^{ipt+i\xi x-\alpha f}d\xi\,,$$

where $F(\xi)=(2\xi^2-k^2)^2-4\alpha\beta\xi^2$,

$$\alpha^2=\xi^2-h^2\,,\quad \beta^2=\xi^2-k^2\,,\quad k=p\sqrt{\frac{\rho}{\mu}}=\frac{p}{V_s}\,. \tag{2.2}$$

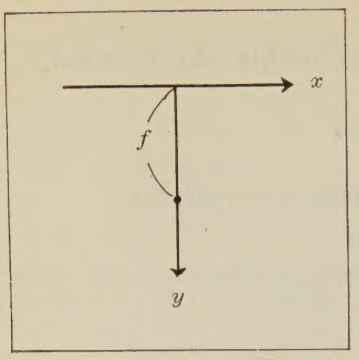

Fig. 1.

In order to satisfy the radiation condition (SOMMERFELD. A: 1949, p, 189) at $x\to\infty$, we must have

the real parts of α and $\beta>0$. (2.3)

We can satisfy these conditions by interpreting the integral expressions for u and v in (2.2) as the limits of the contour integrals

$$u(x, y=0, t) = 2ik^2\int_L \frac{\zeta\sqrt{\zeta^2-k^2}}{F(\zeta)} e^{ipt+i\zeta x-f\sqrt{\zeta^2-h^2}}\,d\zeta,$$

$$v(x, y=0, t) = k^2\int_L \frac{2\zeta^2-k^2}{F(\zeta)} e^{ipt+i\zeta x-f\sqrt{\zeta^2-h^2}}\,d\zeta,$$

$$F(\zeta)=(2\zeta^2-k^2)^2-4\zeta^2\sqrt{\zeta^2-h^2}\sqrt{\zeta^2-k^2} \tag{2.4}$$

when semi-circles around six singular points $\pm h$, $\pm k$ and $\pm\kappa$ are made vanishingly small and $\sqrt{\zeta^2-h^2}$ and $\sqrt{\zeta^2-k^2}$ at the right end of L are assumed to be positive real.

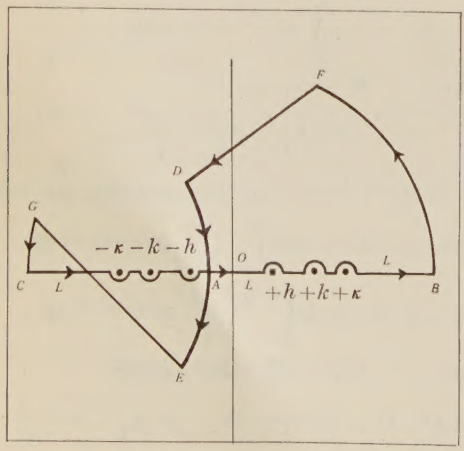

Fig. 2.

In Fig. 2, $\pm\kappa$ are the poles of the integrands in (2.4) for which

$$F(\pm\kappa)=0. \tag{2.5}$$

In order to calculate u and v in (2.4) by the method of contour integral, we shall integrate the integrands in (2.4) on the path $L+(B\to F\to D\to A\to E\to G\to C)$, where BF and GC are parts of a large circle with the center at the origin O and $D\to A\to E$ is the path on which

$$Z=i\zeta x-f\sqrt{\zeta^2-h^2} \tag{2.6}$$

in (2.4) is pure imaginary, and on FD or EG, the imaginary part of $i\zeta x-f\sqrt{\zeta^2-h^2}$ is kept the same as that at D or E. The points D and E are made far away from A in the following analysis. Since there is no singular point inside the path and since the integrands vanish on BF and GC, we may replace the integrals on the right-hand sides of (2.4) by those on $G\to E\to A\to D\to F$. In the following analysis, some physical reasons will be given why we may omit the contributions from the paths $G\to E$ and $D\to F$. Thus we have

$$u(x, y=0, t) = 2ik^2\int_{E\to A\to D} \frac{\zeta\sqrt{\zeta^2-k^2}}{F(\zeta)} e^{ipt+i\zeta x-f\sqrt{\zeta^2-h^2}}\,d\zeta,$$

$$v(x, y=0, t) = k^2\int_{E\to A\to D} \frac{2\zeta-k^2}{F(\zeta)} e^{ipt-i\zeta x-f\sqrt{\zeta^2-h^2}}\,d\zeta. \tag{2.7}$$

§ 3. In order to transform (2.7) into more convenient forms for numerical calculations, we shall make some mathematical considerations in the present section.

(a) At first, it can easily be shown that the coordinate ζ at A and Z in (2.6) there are

$$\zeta=-\frac{hx}{r}, \quad Z=-ihr, \quad r=\sqrt{x^2+y^2}, \tag{3.1}$$

respectively.

(b) ζ, $\sqrt{\zeta^2-h^2}$ and $\sqrt{\zeta^2-k^2}$ on AD are of the forms $-(+)+i(+)$, where $(+)$'s are some positive real numbers. ζ on AE is the complex conjugate of that on AD, and $\sqrt{\zeta^2-h^2}$ and $\sqrt{\zeta^2-k^2}$ on AE are $-$(complex conjugates) of those on AD, respectively.

(c) $Z=i\zeta x-f\sqrt{\zeta^2-h^2}$ on AD and AE can be put

$$Z=-ihr\cosh\phi\ ,\quad 0\leqq\phi\leqq+\infty\ , \tag{3.2}$$

where

$$\zeta=\frac{h}{r}(-x\cosh\phi\pm if\sinh\phi)\ ,$$

$$d\zeta=\pm\sqrt{\zeta^2-h^2}\,d\phi\ , \tag{3.3}$$

respectively.

(d) By means of (3.3), (2.7) is transformed into

$$u(x,\,y=0,\,t)=4k^2\int_0^\infty iU_1(\zeta)e^{i(pt-kr\cosh\phi)}d\phi,$$

$$v(x,\,y=0,\,t)=2k^2\int_0^\infty iV_2(\zeta)e^{i(pt-kr\cosh\phi)}d\phi, \tag{3.4}$$

where U_1 and V_2 are the real and imaginary parts of $\dfrac{\zeta\sqrt{\zeta^2-h^2}\sqrt{\zeta^2-k^2}}{F(\zeta)}$ and $\dfrac{\sqrt{\zeta^2-h^2}(2\zeta^2-k^2)}{F(\zeta)}$ on AD, respectively.

(e) Putting

$$\zeta=pa\zeta',\quad h=pa=\frac{p}{V_p},\quad k=pb=\frac{p}{V_s}=mpa,$$

$$m=\frac{b}{a} \tag{3.5}$$

and assuming $S(t)$ instead of e^{ipt} in (2.1) for the time variations of the displacement and stress near the origin, we have

$$u=4\frac{b^2}{a}\int_0^\infty U_1(\zeta')S'(t-ar\cosh\phi)d\phi,$$

$$v=2\frac{b^2}{a}\int_0^\infty V_2(\zeta')S'(t-ar\cosh\phi)d\phi, \tag{3.6}$$

where S' means the differentiation with respect to the argument in the bracket.

(f) The radial displacement u_R and radial stress T_{RR} in the immediate neighbourhood of the wave origin are given by (2.1) as

$$u_R=\frac{S(t)}{R}\ ,\quad T_{RR}=-\frac{2\mu}{R^2}S(t). \tag{3.7}$$

In the following numerical calculations, we shall assume

$$S(t)=0\ ,\quad -\infty<t<0\ ,\quad S(t)=\text{const.},\quad t\geqq0$$

or

$$S'(t)=0,\quad t\gtrless0,$$

$$S'(t)=\infty\ ,\quad S'(t\,dt=S,\ \text{say at } t=0. \tag{3.8}$$

This is nothing but the time variation assumed in Lapwood's paper.

(g) For the time variation in (3.8), we have

$$u(x,\,y=0,\,t)=4m^2\,{}_f^S\,{}_r^f\begin{pmatrix}U_1(\zeta')\\ \sinh\phi\end{pmatrix}_{\cosh\phi=\frac{t}{ar}=\frac{t}{r/V_p}},$$

$$v(x,\,y=0,\,t)=2m^2\,{}_f^S\,{}_r^f\begin{pmatrix}V_2(\zeta')\\ \sinh\phi\end{pmatrix}_{\cosh\phi=\frac{t}{r/V_p}},$$

$$0\leqq\phi<\infty, \tag{3.9}$$

where

$$m=\frac{b}{a}=\frac{V_p}{V_s}\ ,\quad r=\sqrt{x^2+f^2}\ ,$$

$$\zeta'=\frac{1}{r}(-x\cosh\phi+if\sinh\phi) \tag{3.10}$$

and $U_1(\zeta')$ and $V_2(\zeta')$ are

$$\text{the real part of } \frac{\zeta'\sqrt{\zeta'^2-1}\sqrt{\zeta'^2-m^2}}{F(\zeta')}$$

$$\text{the imaginary part of } \frac{\sqrt{\zeta'^2-1}(2\zeta'^2-m^2)}{F(\zeta')} \tag{3.11}$$

on AD, respectively. In (3.11), $F(\zeta')$ denotes

$$F(\zeta')=(2\zeta'^2-m^2)^2-4\zeta'^2\sqrt{\zeta'^2-1}\sqrt{\zeta'^2-m^2} \tag{3.12}$$

and it is to be noted that the real and imaginary parts of $\sqrt{\zeta'^2-1}$ or $\sqrt{\zeta'^2-m^2}$ on AD are negative and positive, respectively. (3.9)–(3.12) are the formulas by which we can calculate the horizontal and vertical displacements on the free surface for the wave origin (3.7) and (3.8). The displacements are calculated for the non-dimensional independent variables $\dfrac{x}{f}$ and $\dfrac{t}{ar}=\dfrac{t}{r/V_p}$ which are the horizontal distance referred to the depth of the wave origin and the time referred to the time of transit of P wave across the distance $r=\sqrt{x^2+f^2}$.

§ 4. In our numerical examples, we assumed

$$\lambda=\mu\ ,\quad m=\frac{b}{a}=\frac{V_p}{V_s}=\sqrt{3} \tag{4.1}$$

and calculated the displacements at $\dfrac{x}{f}=0$, 1, 2, 3, 5, 10, 20 and 50. ${}_S^f u$ and ${}_S^f v$ thus calculated are shown in Fig. 3.

The results to be noted are as follows:

(a) As it should be, there is no displace-

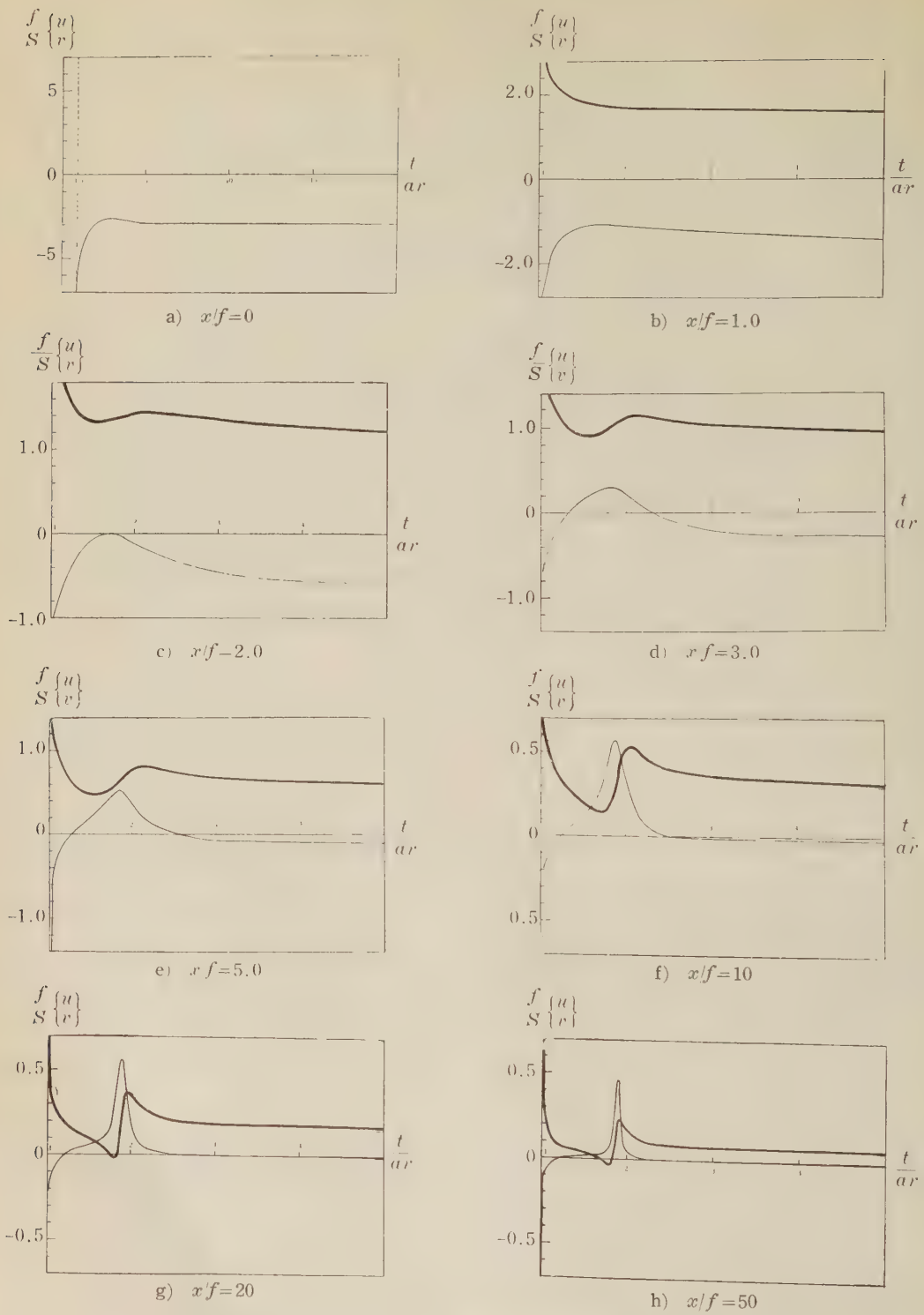

Fig. 3. thich line: $\frac{f}{S}u$, thin line: $\frac{f}{S}v$

ment before the time $t=\frac{r}{V_p}$.

(b) Horizontal displacement u at $x=0$ is zero all through the time. This will be understood by the consideration of symmetry as shown in Fig. 4. Vertical displacement at

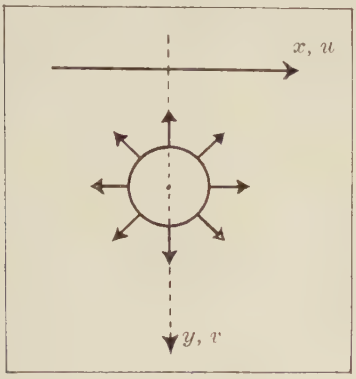

Fig. 4.

$x=0$ is a sudden upward motion corresponding to the P phase followed by a gradual decrease to a permanent displacement.

(c) Vertical displacement v at $x=f$ is very similar to that at $x=0$. u at this point is a sudden outward motion corresponding to the P phase followed by a gradual decrease to a permanent displacement. There is neither S phase nor RAYLEIGH phase in the displacements at $x=0$ and f.

(d) In the displacements at $x\geq 2f$, there appears a phase corresponding to the RAYLEIGH wave. The time in which the RAYLEIGH wave traverses the distance x is $t=\frac{x}{V_R}=1.88\frac{x}{V_p}\fallingdotseq 1.88\frac{r}{V_p}$. Corresponding to this time there is a maximum in the vertical displacement v. In view of these results, we may say that the RAYLEIGH wave appears at about $x=2f$.

(e) There is no S phase in any of our figures. This seems to be inconsistent with the result obtained by LAPWOOD. Thus, in Fig. 22-(a) in LAPWOOD's paper which concerns with the same problem as ours, we see a phase corresponding to the S wave. This contradiction, however, may be settled as follows. As was said in section 1, LAPWOOD obtained the expressions for the component displacements corresponding to the P, S and RAYLEIGH waves. It is these component waves which are shown in his figure above cited. In order to get the total displacement at any time, he must sum up the contribution from each component wave. He did not make this summing-up process. On the other hand, as our method of treating the problem is entirely different from LAPWOOD's, it is not necessary in our analysis to make the summations. Thus, it may be that LAPWOOD's S phase is masked by his RAYLEIGH wave, say, in the course of the summing-up process, and on making the summation, LAPWOOD's results agree completely with ours. In order to ascertain this point, using his formulas for the component waves, we calculated the amplitudes of his S and RAYLEIGH waves at the time when the S component wave takes its maximum amplitude. The amplitude of the RAYLEIGH wave at this time turned out to be about 10 times that of the S wave. Thus our inference was shown to be correct.

(f) Putting t, $x\to\infty$ in (3.9)-(3.12), we get the following expressions for the permanent displacements at points far away from the wave origin

$$\begin{matrix} f \\ S \end{matrix} u\to 3\frac{f}{r}, \quad v\to 0. \tag{4.2}$$

These asymptotic values are shown in the figures for $\frac{x}{f}=10$, 20 and 50 in Fig. 3. From

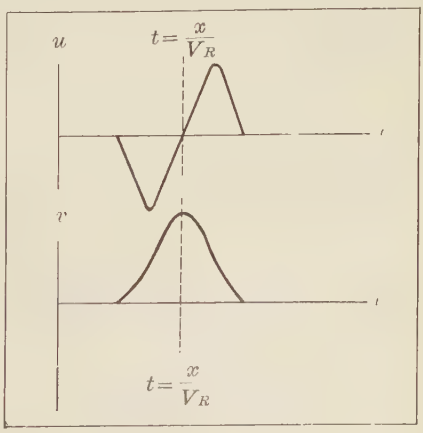

Fig. 5.

these figures, we see that around these asymptotic values, the RAYLEIGH waves take their typical forms as shown in Fig. 5. As to the asymptotic values themselves, they must coincide with the statical deformations due to a statical compressional line source at the depth f. This kind of problem was studied by B. JEFFREY (1921) using bipolar coordinates, and our results can be shown to agree with his results. Anyway, it is rather surprising that the permanent displacements are of the same orders of magnitude as the amplitudes of the RAYLEIGH waves for the step-function type time variation at the wave origin.

(g) u and v in (3.9) at a certain t denote the elementary waves which arrive at the observing point at this time. Since t in (3.9) is between $t=\frac{r}{V_v}$ and $t=\infty$, (3.9) covers the whole plausible time interval. Furthermore, as was said before, the permanent displacements in (4.2) were shown to agree with the statical deformations for the statical compressional origin. In view of these results, it may be justified to omit the contributions from the paths $G\to E$ and $D\to F$ in getting (2.7).

(h) Recently, using agar-agar as an elastic medium, K. KASAHARA (1955) has made the experimental study of the present problem. His results agree faily well with those obtained above.

§ 5. In the similar way as above, we can study the surface displacements due to a distortional line source. It was shown by H. NAKANO (1925) that for the distortional line source

$$u_0=\frac{\partial\psi}{\partial y}\,,\quad v_0=-\frac{\partial\psi}{\partial x}\,,$$

$$\psi=\frac{\pi i}{2}e^{ipt}H_0^{(2)}(kR)=-\int_0^\infty e^{i(pt-kR\cosh\phi)}d\phi\,,$$

where

$$R^2=x^2+(y-f)^2\,,\quad k=p\sqrt{\frac{\rho}{\mu}}=\frac{p}{V_s} \tag{5.1}$$

at a depth f, we have

$$u(x,y=0,t)=k^2\int_L\frac{2\zeta^2-k^2}{F(\zeta)}e^{ipt+i\zeta x-f\sqrt{\zeta^2-k^2}}d\zeta\,,$$

$$v(x,y=0,t)=-2ik^2\int_L\frac{\zeta\sqrt{\zeta^2-k^2}}{F(\zeta)}e^{ipt+i\zeta x-f\sqrt{\zeta^2-k^2}}d\zeta\,,$$

$$F(\zeta)=(2\zeta^2-k^2)^2-4\zeta^2\sqrt{\zeta^2-h^2}\sqrt{\zeta^2-k^2}\,, \tag{5.2}$$

where L denotes the path shown in Fig. 2. Deforming the path of integration as in section 3, we get the following results which correspond to (3.7)-(3.12).

$$u_\theta(R\to 0)=-\frac{S(t)}{R}\,,\quad T_{\theta R}(R\to 0)=\frac{2\mu S(t)}{R^2}\,. \tag{5.3}$$

$$S(t)=0\,,\quad -\infty<t<0\,;\quad S(t)=\text{const.}\,,\quad t\geq 0\,. \tag{5.4}$$

$$S'(t)=0\,,\quad t\neq 0\,,$$

$$S'(t)=\infty\,,\quad S'(t)dt=S\,,\quad t=0. \tag{5.5}$$

$$u(x,y=0,t)=2\frac{S}{f}\frac{f}{r}\begin{pmatrix}V_1(\zeta')\\ \sinh\phi\end{pmatrix}_{\cosh\phi=\frac{t}{br}=\frac{t}{r/V_s}}\,,$$

$$v(x,y=0,t)=-4\frac{S}{f}\frac{f}{r}\begin{pmatrix}U_2(\zeta')\\ \sinh\phi\end{pmatrix}_{\cosh\phi=\frac{t}{br}=\frac{t}{r/V_s}}\,,$$

$$0\leq\phi<\infty. \tag{5.6}$$

$$\zeta'=\frac{1}{r}(-x\cosh\phi+if\sinh\phi)\,,\quad r=\sqrt{x^2+f^2}. \tag{5.7}$$

$V_1(\zeta')$ and $U_2(\zeta')$ in (5.6) are

$$\text{the imaginary part of }\frac{(2\zeta'^2-1)\sqrt{\zeta'^2-1}}{F(\zeta')}$$

$$\text{the real part of }\frac{\zeta'\sqrt{\zeta'^2-1}\sqrt{\zeta'^2-m'^2}}{F(\zeta')} \tag{5.8}$$

on AD, respectively. In (5.8)

$$F(\zeta')=(2\zeta'^2-1)^2-4\zeta'^2\sqrt{\zeta'^2-1}\sqrt{\zeta'^2-m'^2}\,,$$

$$m'=\frac{1}{m}=\frac{a}{b}=\frac{V_s}{V_p} \tag{5.9}$$

and it is to be noted that the real and imaginary parts of $\sqrt{\zeta'^2-1}$ or $\sqrt{\zeta'^2-m'^2}$ on AD are negative and positive, respectively. In the case of the distortional origin, there is one more point to be considered. When

$$\frac{kx}{r}>h\ \text{ or }\ x>\frac{hf}{\sqrt{k^2-h^2}}=\frac{V_sf}{\sqrt{V_p^2-V_s^2}}\,, \tag{5.10}$$

the point A comes to the left-hand side of $\zeta=-h$ as in Fig. 6, and the singular point $\zeta=-h$ is included in the path of integration $L\to B\to F\to D\to A\to E\to G\to C$. In order to get rid of the difficulties thus caused, we shall

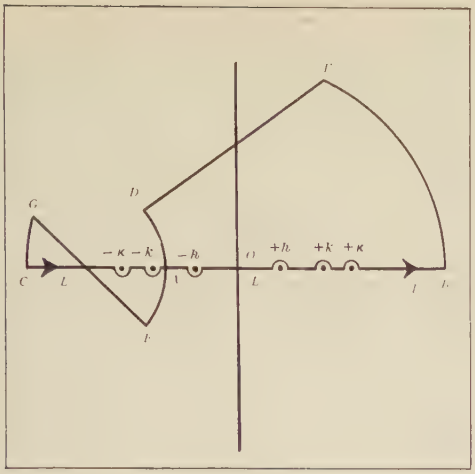

Fig. 6.

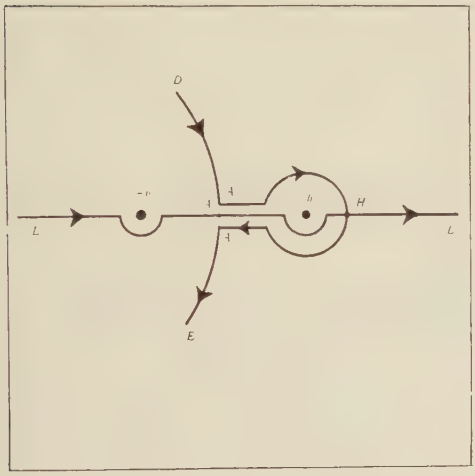

Fig. 7.

consider the integral along the path $L\to B\to F\to D\to A_2\to H\to A_1\to E\to G\to C$ in Fig. 7. Since there is no singular point inside this new path, we can rewrite (5.2) as follows.

$$u(x,y=0,t)=k^2\left(\int_{EA_1+A_2D}+\int_{A_1H}-\int_{A_2H}\right)\times\frac{2\zeta^2-k^2}{F(\zeta)}e^{ipt+i\zeta x-f\sqrt{\zeta^2-k^2}}d\zeta\,,$$

$$v(x,y=0,t)=-2ik^2\left(\int_{EA_1+A_2D}+\int_{A_1H}-\int_{A_2H}\right)\times\frac{\zeta\sqrt{\zeta^2-h^2}}{F(\zeta)}e^{ipt+i\zeta x-f\sqrt{\zeta^2-k^2}}d\zeta\,. \tag{5.11}$$

The integrations along the path EA_1+A_2D can be reduced to the same formulas as in (5.6)–(5.9) and those along the path A_1H-A_2H are transformed into

$$u(x,y=0,t)\text{(additional)}=8m^2\frac{S}{f}\frac{f}{x}\frac{\xi^2(2\xi^2-m^2)(\xi^2-1)^{1/2}(m^2-\xi^2)^{1/2}}{G(\xi)}\,,$$

$$v(x,y=0,t)\text{(additional)}=4m^2\frac{S}{f}\frac{f}{x}\frac{\xi(\xi^2-1)^{1/2}(2\xi^2-m^2)^2}{G(\xi)}\,,$$

$$G(\xi)=[(2\xi^2-m^2)^4+16\xi^4(\xi^2-1)(m^2-\xi^2)]\times\left[1-\frac{f}{x}\frac{\xi}{(m^2-\xi^2)^{1/2}}\right],$$

$$m\frac{x}{r}\geq\xi\geq1\,,\quad \frac{t}{ax}=\frac{t}{x/V_p}=\xi+\frac{f}{x}(m^2-\xi^2)^{1/2}\,,$$

$$(\xi^2-1)^{1/2}\,,\quad (m^2-\xi^2)^{1/2}=+\text{real}. \tag{5.12}$$

The time at which these additional displacements begin are given by

$$t=ax+af(m^2-1)^{1/2}=\frac{x}{V_p}+\frac{f}{V_pV_s}\sqrt{V_p^2-V_s^2}$$

$$=\frac{f}{V_s\cos\Theta}+\frac{x-f\tan\Theta}{V_p}=\frac{OA}{V_s}+\frac{AB}{V_p}\,,$$

$$\sin\Theta=\frac{V_s}{V_p}. \tag{5.13}$$

This is the time corresponding to a kind of surface P wave which occurs at point A in Fig. 8. From Fig. 8, it can easily be understood that we must have the condition (5.10) for the occurrence of this wave.

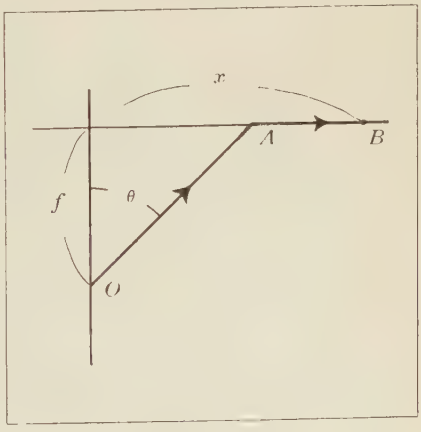

Fig. 8.

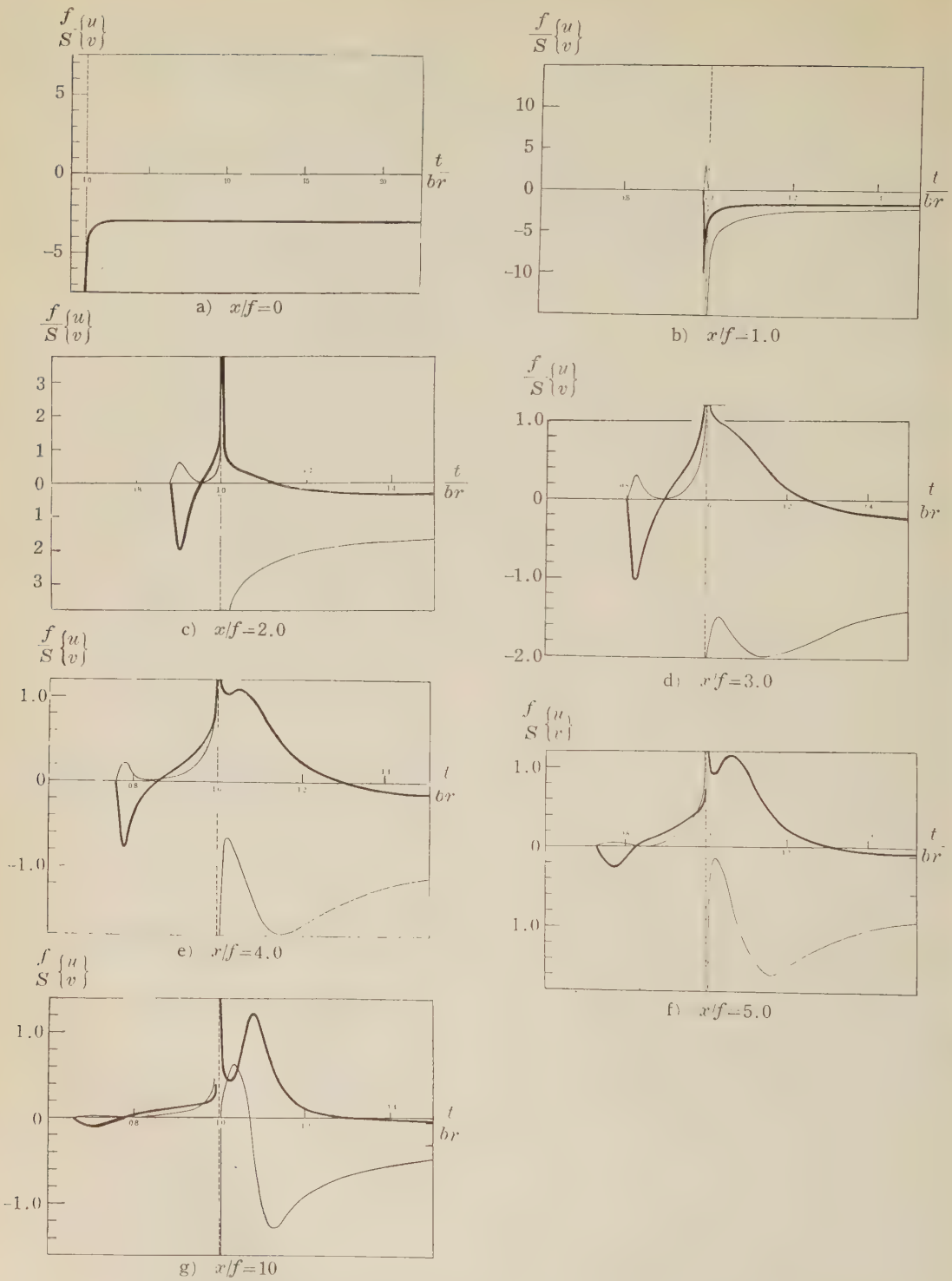

Fig. 9. thich line: $\frac{f}{S}u$, thin line: $\frac{f}{S}v$

§ 6. Using (5.6)–(5.9) and (5.12) and putting

$$\lambda=\mu\ ,\quad m^2=3\ ,\quad m'^2=\frac{1}{3} \tag{6.1}$$

as before, we calculated the displacements at $\frac{x}{f}=0,\ 1,\ 2,\ 3,\ 4,\ 5$ and 10. The results obtained are shown in Fig. 9. The results to be noted are as follows:

(a) Vertical displacement v at $x=0$ is zero all through the time. This will be understood by the consideration of symmetry as shown in Fig. 10. Horizontal displacement u at $x=0$

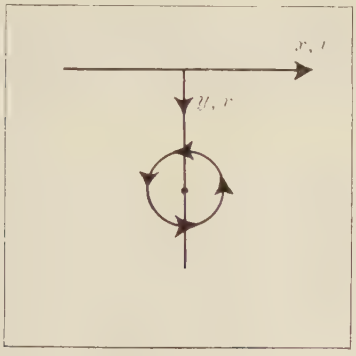

Fig. 10.

is a sudden inward motion corresponding to the S phase followed by a gradual decrease to a permanent displacement.

(b) At $x=f$, we can see the surface P wave corresponding to (5.12) and (5.13). The time $\frac{t}{br}=\frac{t}{r/V_s}$ for this wave is smaller than 1. There is no RAYLEIGH phase in the displacements at this point.

(c) In the displacements at $x\geq 3f$, we can see the RAYLEIGH phases. The time in which the RAYLEIGH wave traverses the distance x is $t=\frac{x}{V_R}=1.09\frac{x}{V_s}=1.09\frac{r}{V_s}$. Corresponding to this time $\frac{t}{r/V_s}\fallingdotseq 1.09$, there is a maximum in the horizontal displacement u. In view of these results, we may say that the RAYLEIGH wave appears at about $x=3f$.

(d) Against the results for the compressional origin, there are S phases in any of our figure for the distortional line source.

(e) Putting $t,\ x\to\infty$ in (5.6)–(5.9), we get the following expressions for the permanent displacements at points far away from the origin

$$\underset{S}{f}\ v\to -3\frac{f}{r}\ ,\quad u=0. \tag{6.2}$$

Comparing (6.2) with (4.2), it seems rather strange that we have the permanent vertical (or horizontal) displacement larger than the horizontal (or vertical) one for the distortional (or compressional) wave origin. This question, however, may be settled if we consider that at $r\to\infty$, the radius vector from the wave origin to the observing point is almost parallel with the free surface.

(f) The asymptotic values in (6.2) are shown in the figures for $x=5f$ and $x=10f$ in Fig. 9. From these figures, we see that around these asymptotic values, the RAYLEIGH waves take their typical forms shown in Fig. 5, with u and v interchanged.

References

KASAHARA, K.:
1955 "Experimental studies on the mechanism of generation of elastic waves V" Bull. Earthq. Res. Inst.

LAMB, H.:
1904 "On the propagation of tremors over the surface of an elastic solid" Phil. Trans., A 203, 1.

JEFFREY, G, B.:
1921 "Plane stress and plane strain in bi-polar coordinates" Phil Trans., A 221, 265.

LAPWOOD, E, R.:
1949 "The disturbance due to a line source in a semi-infinite elastic medium" Phil. Trans., A 242, 63.

NAKANO, H.:
1925 "On Rayleigh wave" Jap. J. Astr. Geophys., 2, 233.

SOMMERFELD, A.:
1949 Partial differential equations in physics. Academic Press Inc., New York.

Propagation of Tremors over the Surface of an Elastic Solid.

By
Naota KOBAYASHI
Department of Precision Mechanics, Faculty of Technology, Chūō University, Tokyo.
and
Hitoshi TAKEUCHI
Geophysical Institute, Faculty of Science, Tokyo University, Tokyo.

Abstract

Wave phenomena, which are seen over the surface of a semi-infinite elastic solid subjected to an impulsive line force of SV and SH type, have been studied. The results obtained for the SV type origin are almost the same as for the dilatational origin. In the case of SH type origin, there is neither P wave nor RAYLEIGH wave in seismograms to be obtained.

§ 1. In a previous paper (H. TAKEUCHI and N. KOBAYASHI, 1954), under the same title as above, wave phenomena, which are seen along the surface of a semi-infinite elastic solid subjected to an impulsive force normal to the surface, were studied. In that paper, we got two formulus by which the surface displacements at any point and at any time can be calculated. By using these formulus, we could calculate the surface displacements in the neighbourhood of the wave origin and thus could make clear the way of appearence of RAYLEIGH waves which are the main parts of the displacements at points far away from the wave origin. In the present paper, we shall study the similar problem for a semi-infinite elastic solid subjected to an external tangential force. The tangential force is assumed to be acting at $(x=0, y=0)$ in the rectangular coordinates shown in Fig. 1. There are two types of tangential forces acting at $(x=0, y=0)$. In the so-called *SV* type of tangential wave origin, the force is acting parallel to the x axis. On the other hand, in the so-called SH type of tangential wave origin, the force is acting parallel to the z axis. In 1904, H. LAMB studied the case of tagential wave origin of *SV* type and obtained the formal expressions for the displacements but he did not work out the results in detail. On the other hand, an experimental study for the tangential wave origin has recently been made by NORTHWOOD and ANDERSON (1953). In their paper, they said that when the force is of *SV* type, the result is not so different from that for the normal wave origin. When the force is of *SH* type, however, the result obtained is entirely different from those for the above two cases. For example, there is neither *P* wave nor RAYLEIGH wave in the seismograms for the *SH* type wave origin. To study why these things occur will be one of the main objects of the present paper.

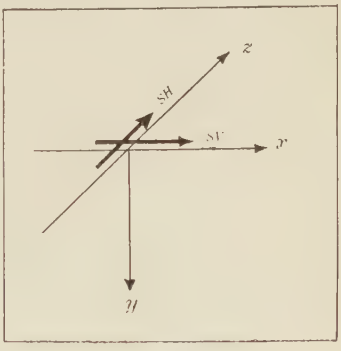

Fig. 1.

§ 2. It was shown by H. LAMB (1904, his equation 55) that the horizontal and vertical displacement u_0 and v_0 at $(x, y=0, t)$ due to

a SV type tangential force $Q\,e^{ipt}$ acting at $(x=0,\ y=0)$ are given by

$$u_0=-\frac{Q}{2\pi\mu}\int_{-\infty}^{+\infty}\frac{k^2\sqrt{\xi^2-k^2}}{F(\xi)}e^{i(pt+\xi x)}d\xi,$$

$$v_0=i\frac{Q}{2\pi\mu}\int_{-\infty}^{+\infty}\frac{\xi(2\xi^2-k^2-2\sqrt{\xi^2-h^2}\sqrt{\xi^2-k^2})}{F(\xi)}\times e^{i(pt+\xi x)}d\xi,$$

where

$$F(\xi)=(2\xi^2-k^2)^2-4\xi^2\sqrt{\xi^2-h^2}\sqrt{\xi^2-k^2}. \quad (2.1)$$

In (2.1), the notations are all the same as in Lamb's paper. In order to satisfy the radiation condition at $x\to\infty$ (A. SOMMERFELD, 1949, p. 189), we must interpret the integrals in (2.1) as the limits of those along the path L_1 in the complex ξ plane shown in Fig. 2 when semicircles around six singular points $\xi=\pm h$, $\pm k$ and $\pm\kappa$ are made vanishingly small. We must also assume that $\sqrt{\xi^2-h^2}$ and $\sqrt{\xi^2-k^2}$ are positive real on the right end of L_1. In order to calculate u_0 and v_0 in (2.1), we shall consider

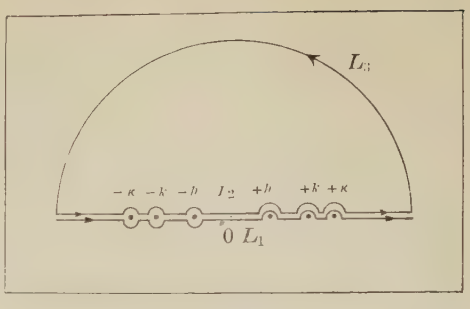

Fig. 2

$$0=-\frac{Q}{2\pi\mu}\int_{L_2+L_3}\frac{k^2\sqrt{\xi^2-k^2}}{F(\xi)}e^{i(pt+\xi x)}\,d\xi,$$

$$0=i\frac{Q}{2\pi\mu}\int_{L_2+L_3}\frac{\xi(2\xi^2-k^2-2\sqrt{\xi^2-h^2}\sqrt{\xi^2-k^2})}{F(\xi)}\times e^{i(pt+\xi x)}. \quad (2.2)$$

L_3 in (2.2) is a large semi-circle with the center at 0. As there is no singular point inside (L_2+L_3), the integrals in (2.2) are equal to zero. Making the differences of the corresponding expressions in (2.1) and (2.2), we get

$$u_0=-\frac{Q}{\pi\mu}\int_h^k\frac{4\xi^2k^2\sqrt{\xi^2-h^2}\sqrt{\xi^2-k^2}}{F(\xi)f(\xi)}e^{i(pt-\xi x)}\,d\xi-\frac{Q}{\pi\mu}\boldsymbol{P}\int_k^\infty\frac{k^2\sqrt{\xi^2-k^2}}{F(\xi)}e^{i(pt-\xi x)}\,d\xi,$$

$$v_0=\frac{Q}{\mu}Be^{i(pt-\kappa x)}-\frac{iQ}{\pi\mu}\int_h^k\frac{2k^2\xi(2\xi^2-k^2)\sqrt{\xi^2-h^2}\sqrt{\xi^2-k^2}}{F(\xi)f(\xi)}e^{i(pt-\xi x)}\,d\xi,$$

$$f(\xi)=(2\xi^2-k^2)^2+4\xi^2\sqrt{\xi^2-h^2}\sqrt{\xi^2-k^2},$$

$$B=-\frac{\kappa(2\kappa^2-k^2-2\sqrt{\kappa^2-h^2}\sqrt{\kappa^2-k^2})}{F(\kappa)}, \quad (2.3)$$

where $\boldsymbol{P}$ denotes the principal value of the integral concerned. u_0 and v_0 in (2.3) are the formal expressions for the horizontal and vertical displacements due to the tangential force Qe^{ipt}.

§3. Putting

$$\xi=pa\theta,\quad h=pa,\quad k=pb,\quad \kappa=pc \quad (3.1)$$

in (2.3) and generalizing the law of time variation of the tangential force at the origin, we get

$$m\pi\mu u_0=\boldsymbol{P}\int_1^\infty U(\theta)Q(t-a\theta x)\,d\theta,$$

$$m\pi\mu v_0=m\pi BQ(t-cx)+\int_1^\infty V(\theta)Q(t-a\theta x)\,d\theta \quad (3.2)$$

for the tangential force $Q(t)$ at $(x=0,\ y=0)$. $U(\theta)$ and $V(\theta)$ in (3.2) are given respectively by

$$U(\theta)=\begin{cases}\dfrac{4m^3\theta^2\sqrt{\theta^2-1}(m^2-\theta^2)}{(2\theta^2-m^2)^4+16\theta^4(\theta^2-1)(m^2-\theta^2)} & \text{for } 1\le\theta\le m,\\[2ex] -\dfrac{m^3\sqrt{\theta^2-m^2}}{(2\theta^2-m^2)^2-4\theta^2\sqrt{\theta^2-1}\sqrt{\theta^2-m^2}} & \text{for } m<\theta,\end{cases}$$

$$V(\theta)=\begin{cases}\dfrac{2m^3\theta(2\theta^2-m^2)\sqrt{\theta^2-1}\sqrt{m^2-\theta^2}}{(2\theta^2-m^2)^4+16\theta^4(\theta^2-1)(m^2-\theta^2)} \\ \qquad \text{for} \quad 1\leq\theta\leq m, \\ 0 \quad \text{for} \quad m<\theta, \end{cases} \tag{3.3}$$

where

$$m=\frac{b}{a}=\frac{V_p}{V_s}, \quad a=\frac{1}{V_p}=\sqrt{\frac{\rho}{\lambda+2\mu}},$$
$$b=\frac{1}{V_S}=\sqrt{\frac{\rho}{\mu}}, \quad c=\frac{1}{V_R}. \tag{3.4}$$

Equation (3.2) is valid for any $x(>0)$ and t. We shall now calculate u_0 and v_0 in the case when

$$Q(t_0)=\text{const } Q, \text{ say for } -\tau\leq t_0\leq\tau$$
$$=0 \quad \text{otherwise.} \tag{3.5}$$

Putting $t=\tau t'$ and $t_0=\tau t_0'$ in (3.2), we have, after a few calculation

$$m\pi\mu u_0=QP\int_{\frac{V_p\tau}{x}(t'-1)}^{\frac{V_p\tau}{x}(t'+1)} U(\theta)\,d\theta,$$

$$m\pi\mu v_0=m\pi BQ\,\delta\left(t'-t_0'-\frac{x}{V_p\tau}\right)$$
$$+Q\int_{\frac{V_p\tau}{x}(t'-1)}^{\frac{V_p\tau}{x}(t'+1)} V(\theta)\,d\theta, \tag{3.6}$$

where δ is the Dirac's function. This is the final formula by which we can calculate the values of u_0 and v_0 at any $x(>0)$ and t.

§ 4. In our numerical examples, we assumed

$$\lambda=\mu, \qquad m=\frac{b}{a}=\frac{V_P}{V_S}=\sqrt{3} \tag{4.1}$$

and calculated at first the values of $U(\theta)$ and $V(\theta)$ in (3.6). They are shown in Fig. 3 and 4. Next, the values of $\frac{m\pi\mu}{Q}u_0$ and $\frac{m\pi\mu}{Q}v_0$ are calculated at $t'=\frac{t}{\tau}=0$, 1, 2 and 5. The results are shown in Fig. 5 and 6. The results to be noted are as follows:

(a) The horizontal displacement is outward almost everywhere. There is, however, a very narrow region of inward displacement. This region is propagated with the velocity of the Rayleigh wave $V_R=0.92V_S$. The origin time of this wave is at $t=-\tau$. This is the time at which the tangential force begins to act on the otherwise free surface.

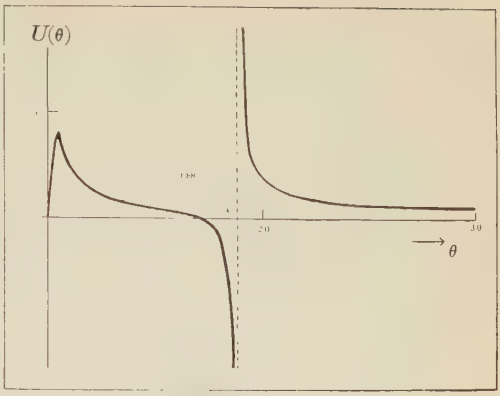

Fig. 3

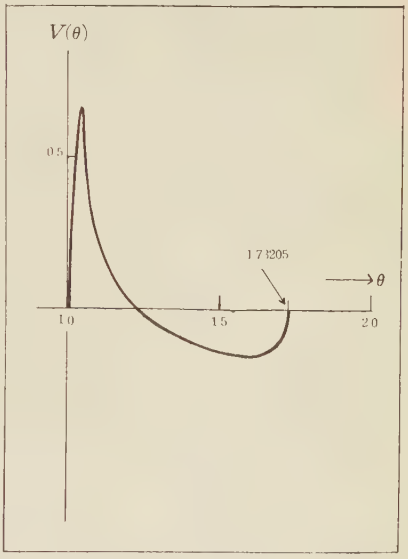

Fig. 4

(b) The fronts of both the horizontal and vertical displacements are propagated with the velocity of P wave V_P. The origin times of these waves are also at $t=-\tau$.

(c) In the horizontal displacements after $t=\tau$, there appears a region of very large outward displacement. This region is propagated with the velocity V_R. The origin time of this wave is at $t=\tau$. This is the time at which the tangential force is removed.

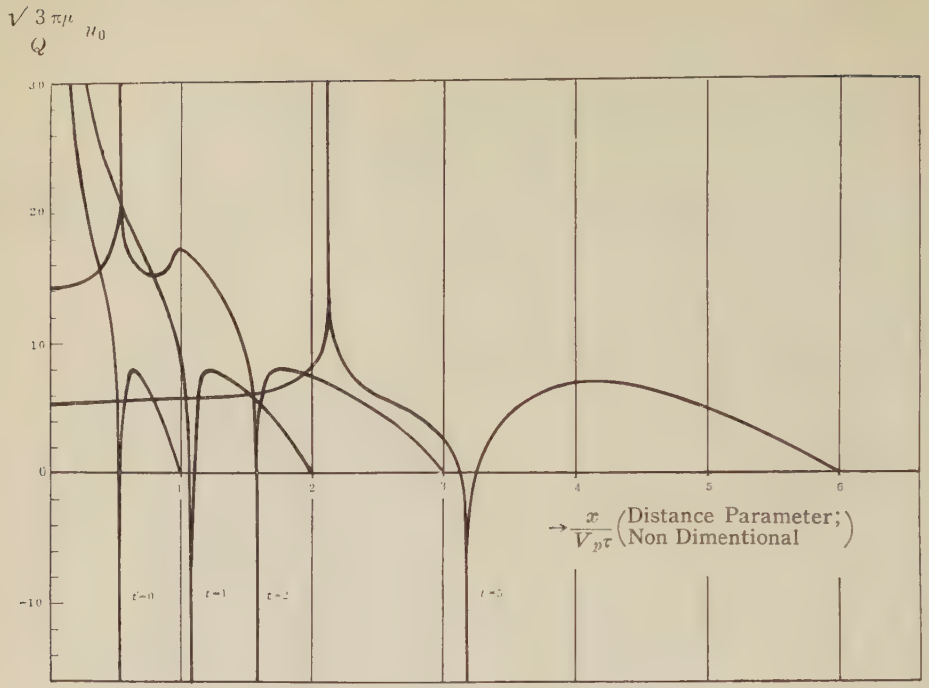
$\sqrt{3}\pi\mu$ u_0
Q
20
10
0
-10
1
2
3
4
5
6
$t=0$
$t=1$
$t=2$
$t=3$
$\rightarrow \frac{x}{V_p\tau}$ (Distance Parameter; Non Dimentional)

Fig. 5

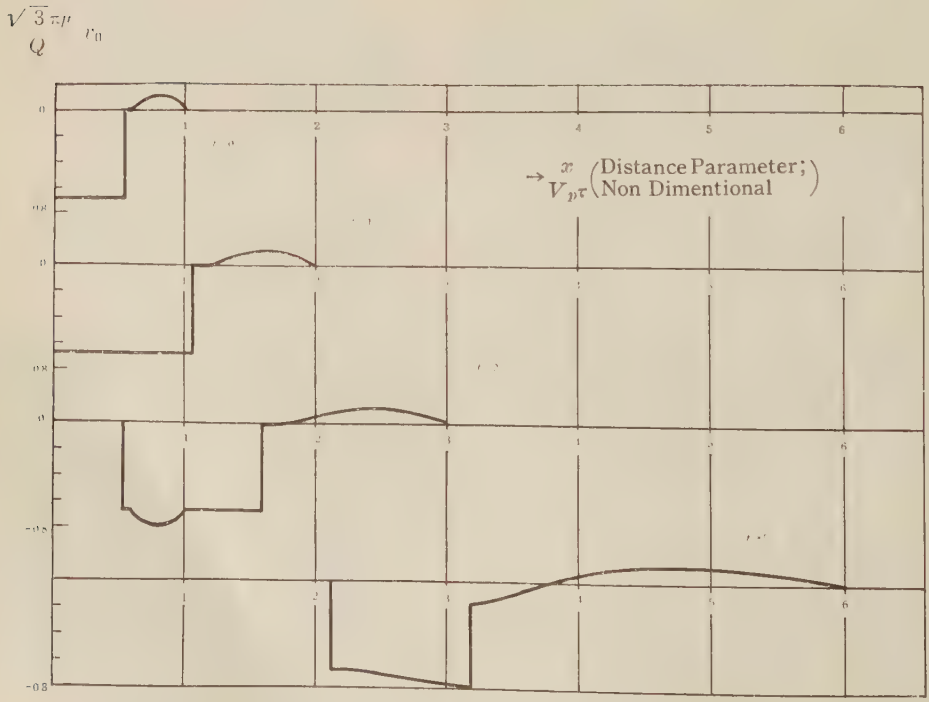
$\sqrt{3}\pi\mu$ v_0
Q
0
1
2
3
4
5
6
$\rightarrow \frac{x}{V_p\tau}$ (Distance Parameter; Non Dimentional)

Fig. 6

(d) The vertical displacement is upward in the domain between the wave front and the point (or rather line) at which the horizontal displacement is a large inward one, and it is downward in the domain between the points at which the horizontal displacements are large inward and outward ones respectively. Thus the domain of downward motion is propagated with the velocity V_R.

(e) The apparent wave length of the generated RAYLEIGH wave is about $2V_P\tau$. This length is approximately equal to the extent of the downward domain at $t=\tau$ at which the tangential force is removed.

(f) The time variations of the displacements at points far away from the wave origin can approximately be obtained by tracing the u_0 and v_0 curves for $t'=5$ in Fig. 5 and 6 from the side of larger $\frac{x}{V_P\tau}$ to that of smaller $\frac{x}{V_P\tau}$.

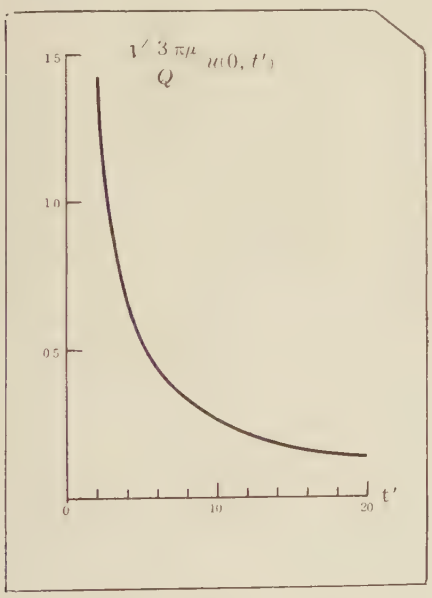

Fig. 7.

(g) The vertical displacement at $x=0$ is zero all through the time. This will be understood from the consideration of symmetry. The horizontal displacement there is a sudden outward motion followed by a gradual decrease to the zero line. It is shown in Fig. 7.

(h) There is no S phase in any of our figures. This result, together with some of the above results, is very similar to that obtained for the compressional wave origin already studied.

§ 5. We shall now study the similar problem for an impulsive tangential origin of SH type. Refering to the rectangular coordinates in Fig. 1, we have the following solutions of the equations of motion for a homogeneous elastic body.

$$u\equiv v\equiv div\vec{u}\equiv 0,$$
$$w=Ae^{i(pt+\xi x)-\beta y}, \qquad \beta^2=\xi^2-k^2,$$
$$k=\frac{p}{V_S}=p\sqrt{\frac{\rho}{\mu}},$$
$$T_{yx}\equiv T_{yy}\equiv 0,$$
$$T_{yz}=\mu\frac{\partial w}{\partial y}=-\mu A\beta e^{i(pt+\xi x)-\beta y},$$
$$w(y=0)=-\frac{1}{\mu\beta}T_{yz}\ (y=0), \tag{5.1}$$

where A is a constant and the real part of β is positive. Thus, for a tangential line source at $x=y=0$, we have

$$w(x,\ y=0,\ t)=w_0, \text{ say}$$
$$=\frac{Q}{2\pi\mu}e^{ipt}\int_{-\infty}^{+\infty}\frac{e^{i\xi x}}{\beta}d\xi,$$
$$Qe^{ipt}=-2T_{yz}(y=0,\ x=0)\,dx. \tag{5.2}$$

Proceeding as in section 2, we can rewrite (5.2) as

$$w_0=\frac{Q}{2\pi\mu}e^{ipt}\left[\int_{-\infty}^{-k}\frac{e^{i\xi x}}{\beta}d\xi-\int_{-\infty}^{-k}\frac{e^{i\xi x}}{-\beta}d\xi\right]$$
$$=\frac{Q}{\pi\mu}e^{ipt}\int_{k}^{\infty}\frac{e^{i(pt-\xi x)}}{\beta}d\xi \tag{5.3}$$

which, for the general type of time variation $Q(t)$, is transformed into

$$w_0=\frac{1}{\pi\mu}\int_1^{\infty}\frac{Q(t-bx\theta)}{\sqrt{\theta^2-1}}d\theta, \tag{5.4}$$

where

$$k=pb, \qquad b=\frac{1}{V_S}, \qquad \xi=pb\theta. \tag{5.5}$$

In the case of an impulsive origin

$$Q(t)=0 \quad \text{for} \quad t>dt,$$

$$Q(t)=\text{const}\ \frac{Q}{dt}\ ,\quad \text{say, for}\quad t<dt, \qquad (5.6)$$

we get

$$w_0=\frac{Q}{\pi\mu bx}\left(\frac{1}{\sqrt{\theta^2-1}}\right),\ \theta=\frac{t}{bx}=\frac{V_S t}{x}\ . \qquad (5.7)$$

(5.7) is the expression for an impulse of S wave type. Thus, in this case, there is neither P wave nor RAYLEIGH wave on seismograms at any point. This result agrees well with the experimental result obtained by NORTHWOOD and ANDERSON. In seismic prospectings, it is very desirable to get some informations on the S wave velocities under the ground. In view of the results above obtained, it is very hopeful to get them along the line studied in this section.

References

LAMB, H.:
1904 "On the propagation of tremors over the surface of an elastic solid" Phil. Trans., A 203, 1.

NORTHWOOD, T. D. and ANDERSON, D. V.:
1953 "Model seismology" Bull. Seis. Soc. Amer., **43**, 239.

SOMMERFELD, A.:
1949 Partial differential equations in physics. Academic Press Inc., New York.

TAKEUCHI, H. and KOBAYASHI, N.:
1954 "Propagation of tremors over the surface of an elastic solid" J. Phys. Earth, **2**, 27.

STONELEY Waves Generated by Explosions.

By
Akira KUBOTERA
Geophysical Institute, Faculty of Science, Kyoto University, Kyoto.

Abstract

Using three components seismometers, field measurements of under ground motions within bore-holes were carried out.

In this experiment, boundary waves which could be considered as STONELEY waves were obtained. The boundary surface is between layers of clay and sand and is of about 9 m depth from the ground surface.

The characteristics of this wave are as follows:

Tne wave velocity is 430 m/sec.

The period of motion is about 0.06 sec.

The particle trajectories are elliptical and retrograde.

The amplitude of the wave is large at the boundary surface and is decreased rapidly on leaving this surface.

These results are in good agreement with those predicted by the classical theory on the STONELEY waves.

§ 1. Introduction

Putting seismometers at various depths within bore-holes, and varying the depth of shot-hole, explosive waves were recorded by vertical and horizontal seismometers.

The most interesting result obtained in these experiments was that the STONELEY wave could be observed by explosions, at the boundary surface between two different layers.

In 1924, R. STONELEY found that it was theoretically possible for RAYLEIGH-type waves to be transmitted along the boundary surface of two elastic solids. Later on, K. SEZAWA and K. KANAI (1938 and 1939) studied mathematically the way of generation of the boundary waves. K. SEZAWA and K. KANAI (1939) and J. G. SCHOLTE (1947) calculated the possible existence range of the STONELEY wave.

Many theoretical studies on the STONELEY wave have been carried out since then. However, there have been no reports on the direct observation of this wave or the opportunities of doing so. (Y. SATO 1953).

In the present experiment, the seismograms recorded a phase which seems to correspond to the boundary wave. This phase could clearly be recorded on the trace of seismograms only when the seismometers were placed at or near the boundary surface of the two different layers.

In view of many other results obtained it seems that this wave corresponds to the STONELEY wave.

§ 2. Experimental Procedure.

Instruments

The instruments employed in these experiments are those used in usual prospecting operations. The seismometers are of the E.T.L. type (Electro-Technical Laboratories' Seismic Detector, Model EVS-3D) with three components (one vertical and two horizontal), the natural frequency being 10 cycle/sec., and the damping being critical. The galvanometers have a natural frequency of 30 cycle/sec., and are critically damped. Each galvanometer is directly connected to a seismometer, with no amplifiers but sometimes with attenuators.

Figure 1 shows a response curve of the entire system, including the seismometer and the galvanometer. The magnification of this system is about 2500 at 20 cycle/sec.

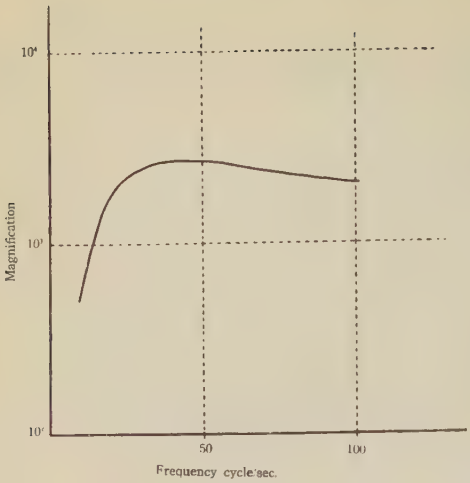

Fig. 1. Frequency-magnification curve for over all system including seismometer, galvonometer and occillograph.

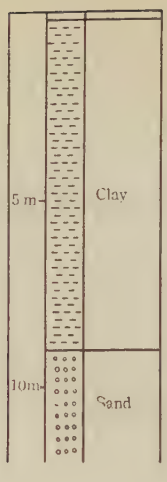

Fig. 2. Geological profile of the test field.

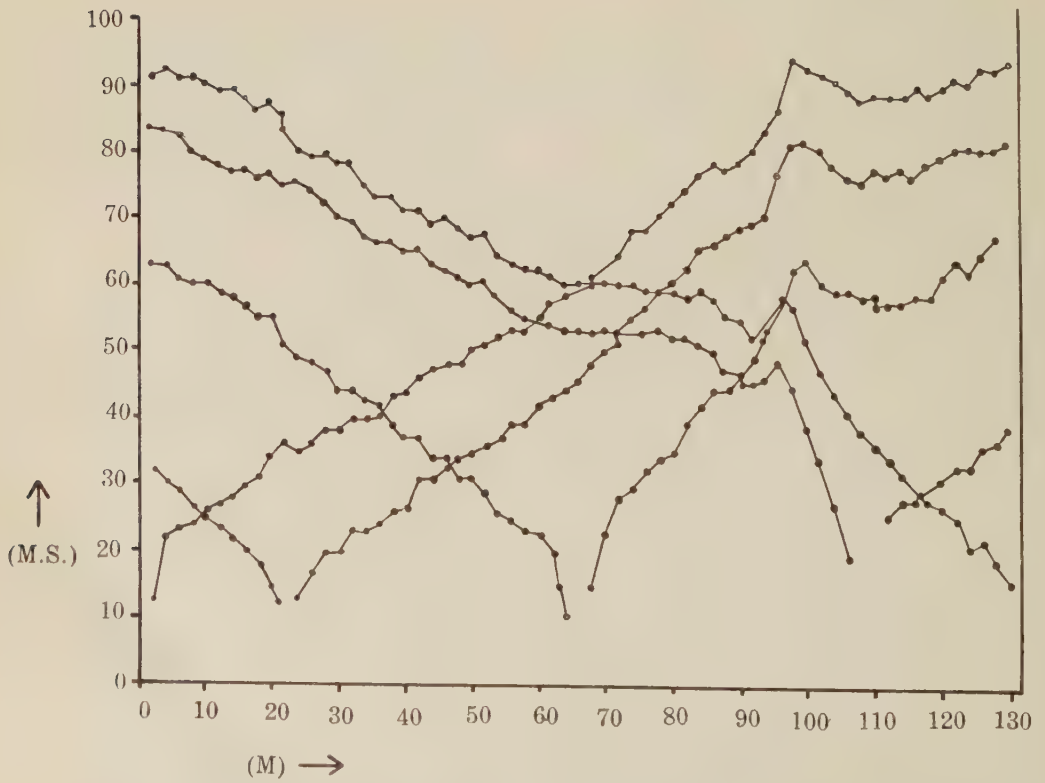

Fig. 3. Time-distance curves by the refraction test. (after T. KAMETANI)

Location

The observations were carried out by the "Seismic Exploration Group of Japan" in Feb. 1954 and March 1955, on the ground of the agricultural field of Tokyo University, Tanashi, Tokyo.

The geological profile here is shown in figure 2. The upper layer is a clay, called "Kanto Loam," under which is a sandy layer beginning 9 m below the surface. The STONELEY wave was observed at the boundary surface between the clay and sand layers.

A seismic prospecting test by the refraction method was carried out in this field by our group, and the result was reported by T. KAMETANI (1954). The time-distance curves in this report are copied in figure 3. The longitudinal wave velocity is gradually increased with the depth. This velocity distribution may be represented by the following formula:

$$v(z)=v_0+az \tag{1}$$

where z is the depth in meter. Using the time-distance curves, the constants v_0 and a are determined as follows:

$$v_0=1411.5\pm3.7 \text{ m/sec.}$$

$$a=32.1\pm1.1 \text{ sec.}^{-1}$$

Shooting procedure

Two types of tests were made as follows: 1) The ground motion resulting from dynamite explosions in a bore-hole of 15 m depth was recorded by seismometers placed at bore-hole bottoms of varying depths. The depths of the seismometer holes were 2 m, 7.5 m, 9.0 m and 10 m in the first test, and 1.5 m, 5.0 m, 8.5 m and 11.5 m in the second test, the shot-receiver distances being 60 m and 45 m in the first and second tests, respectively. (Figure 4)

2) In order to determine the propagation velocity of this wave, three component seismometers (vertical, horizontal radial and horizontal transversal components) were placed at three shot-receiver distances, namely $\Delta=20$m, $\Delta=60$ m and $\Delta=100$ m along the boundary surface of the clay and sand layers, which is at about 9 m depth. An additional instrument was placed at the up-hole 100 m away. A

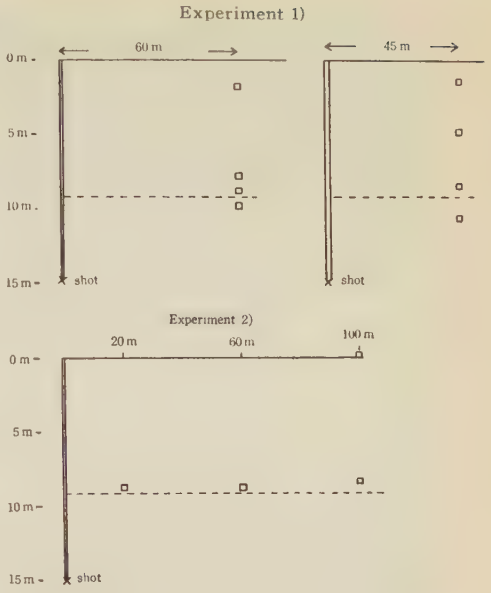

Fig. 4. Maps of disposition of seismometers and shot-holes in the experiment.

dynamite charge was fired at the depth of 15 m under the ground surface.

By using an attenuator, the sensitivity of each seismometer was kept constant in each experiment. The sensitivity of seismometers were changed, however, according to the distance as follows;

Shot-Receiver Distance.	Sensitivity Ratio Vertical	Horizontal
100 m	1	1
60 m	1/3	1
20 m	1/10	1/10

§ 3. Experimental Results.

The seismograms obtained in experiments I and II are shown in figures 5, 6 and 7.

As is seen in figures 5 and 6, there is a remarkable later phase in traces A-1, A-2, B-1 and B-2, but no such phase in trace C, D, E-1 and E-2.

Our conclusion is that this clearly distinguishable later phase is due to a boundary wave, on the ground that it is found near the boundary surface between the clay and sand layers and its amplitude is decreased rapidly on leaving the surface.

Is this wave progressive or not? As shown in figure 7, we found in experiment II that

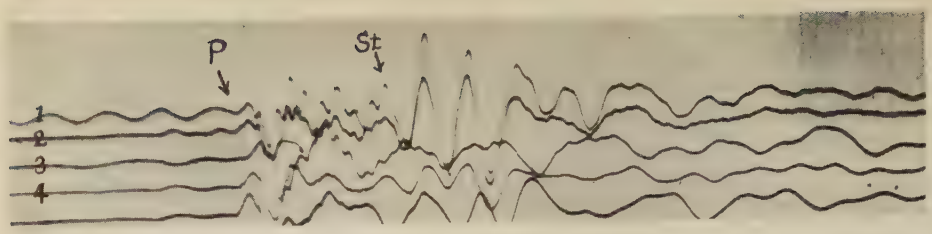

Fig. 5. Seismograms obtained by the 1st test in 1) experiment.

Trace Number	Types of Seismometer	Disposed Depth	Shot-Receiver Distance	Sensitivity Ratio	Notation
1	Vertical 10∞/s.	10 m	60 m	1	A–1
2	〃 〃	9 m	〃	〃	B–1
3	〃 〃	2 m	〃	〃	E–1
4	〃 〃	7½ m	〃	〃	C

(Shot-hole depth; 15 m)

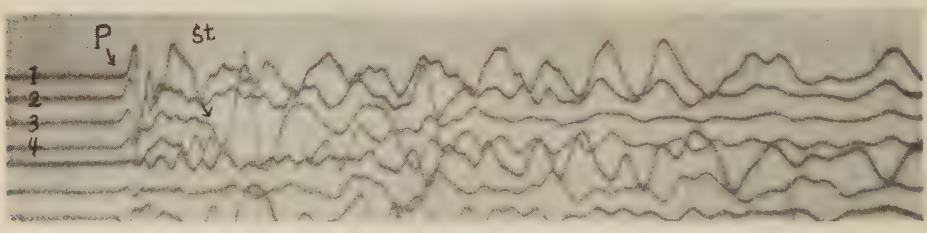

Fig. 6. Seismograms obtained by the 2nd test in 1) experiment.

Trace Number	Types of Seismometer	Disposed Depth	Shot-Receiver Distance	Sensitivity Ratio	Notation
1	Vertical 10∞/s.	1½ m	45 m	1	E–2
2	〃 〃	5 m	〃	〃	D
3	〃 〃	8½ m	〃	〃	B–2
4	〃 〃	11½ m	〃	〃	A–2

(Shot-hole depth; 15 m)

this wave was recorded by the vertical and horizontal radial components of the seismometers at every distance on or near the boundary surface, but not recorded by the up-hole seismometer. Thus, we may safely conclude that this wave propagated along the boundary surface.

In the following paragraphs, some of the characteristics of these boundary waves will be studied.

1) Propagation velocity

The time-distance curves for the initial motions and boundary waves obtained from figure 7 are shown in figure 8. From these time-distance curves, we see that the propagation velocities of the boundary wave and the initial motion are 430 m/sec. and 1800 m/sec., respectively. The propagation velocity of 1800 m/sec. corresponds to the longitudinal wave by the following reason:

By equation (1), the propagation velocities of the longitudinal wave at 9 m (the boundary surface) and 15 m depth (the depth of explosion point) are estimated to be

$$v(z=9)=1728 \text{ m/sec.}$$

$$v(z=15)=1920 \text{ m/sec.}$$

The velocity of 1800 m/sec. lies between these two values.

2) Trajectories of Particle Motions.

Figure 9 shows the particle motion trajectories obtained by the vertical and horizontal

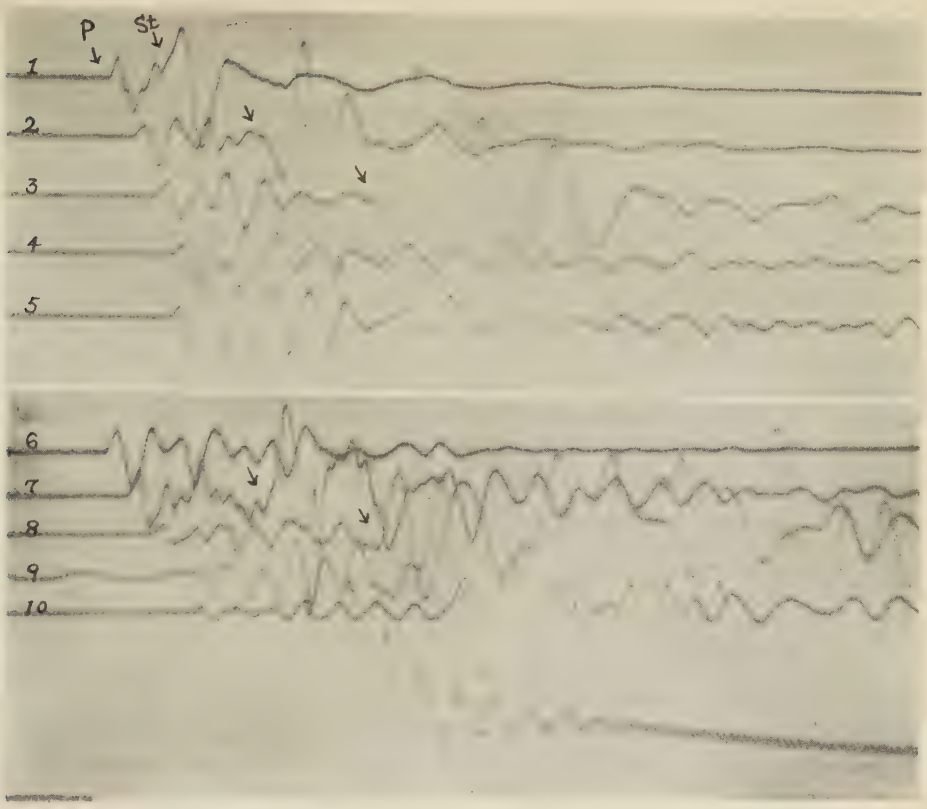

Fig. 7. Seismogram obtained by 2) experiment.

Trace Number	Types of Seismometer	Disposed Depth	Shot-Receiver Distance	Sensitivity Ratio
1	Vertical 10∞/s.	9 m	20 m	1/10
2	〃 〃	9 m	60 m	1/3
3	〃 〃	8½ m	100 m	1
4	〃 〃	0 m	100 m	1
5	〃 27∞/s.	0 m	100 m	—
6	Horizontal 10∞/s.	9 m	20 m	1/10
7	〃 〃	9 m	60 m	1
8	〃 〃	8½ m	100 m	1
9	〃 〃	0 m	100 m	1
10	〃 27∞/s.	0 m	100 m	—

(Shot-hole depth; 15 m)

radial seismometers at a point of 8.5 m depth from the ground surface and 100 m distance from the firing point. Three successive cycles are shown in the figure. The motion is retrograde in the first two cycles and is roughly elliptical, but not so in the third cycle. It seems that the first two cycles correspond to the STONELEY wave but that the third one represents some other type of wave.

At a point of 9 m depth from the ground surface and 60 m from the firing point two cycles can also be seen in trajectories.

3) Period and Dispersion

The period of this wave is about 0.06 sec., but the time intervals between successive peaks and troughs become longer as time

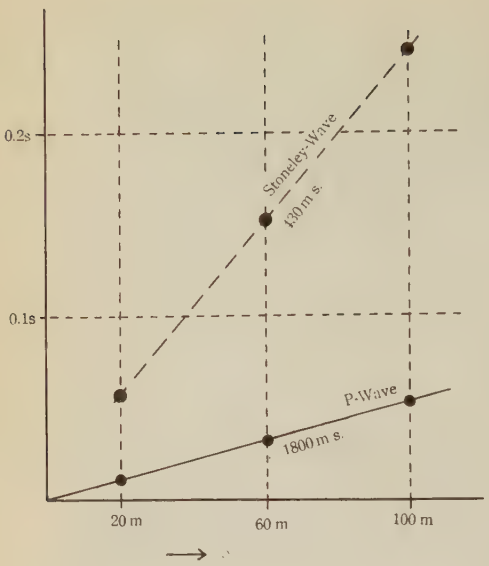

Fig. 8. Time-distance curves for under ground test.

goes on. This time increase may be due to the abnormal dispersion of the wave. The STONELEY wave is not dispersive, if the elastic constants and densities of the two layers are constants. Thus the wave dispersion obtained above may be explained by the complexities of the structure in this region.

4) *Amplitude.*

The amplitude distribution in a vertical column is shown in figure 10. On the other hand, the amplitude distribution versus shot-receiver distance along the boundary surface is shown in figure 11. It is rather difficult to determine the attenuation formula of the STONELEY wave from this figure, because at $\Delta=20$ m, the STONELEY wave is not clearly separated from other waves.

§ 4. Conclusions and Remarks

In this section, the existence conditions and the excitation conditions of the STONELEY wave derived theoretically will be discussed.

K. SEZAWA and K. KANAI (1938) and F. G. SCHOLTE (1947) determined the range of the density ratio (ρ/ρ') and the elastic constant ratio (μ/μ') of two separated layers within which STONELEY waves can be existed. Some of the results obtained are shown in figure 12. From figure 12, we see that the range of

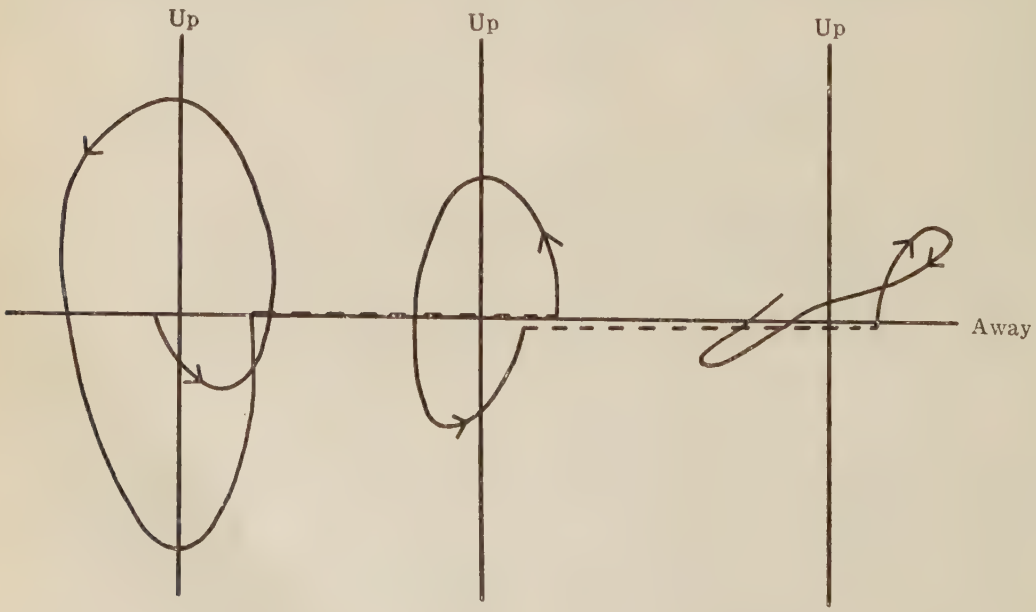

Fig. 9. Particle trajectories of succesive STONELEY wave recorded at 8.5 m deep and 100 m shot-receiver distance.

$\begin{pmatrix} \mu & \rho \\ \mu' & \rho' \end{pmatrix}$ within which the STONELEY waves can be existed is quite narrow. When $\left(\frac{\mu}{\mu'} \Big/ \frac{\rho}{\rho'} \approx 1\right)$, i.e., when the velocity difference of two separated layers is quite small, the STONELEY wave can be existed.

In the present experiment, there was hardly any velocity difference between the two separated layers as was shown in figure 3, although the layers are clearly distinguishable in the bore-hole tests.

Thus it may safely be concluded that in this field, the existence conditions for the STONELEY wave are satisfied.

Next we shall consider the generation condition of the STONELEY wave: K. SEZAWA and K. KANAI (1938 and 1939) showed mathematically that dilatational wave origins or distortional origins of SV type can generate the

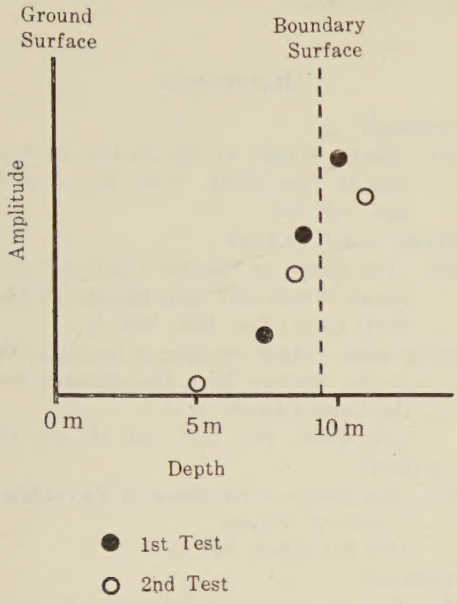

Fig. 10. Effect of depth upon the vertical component of the amplitude of STONELEY waves.

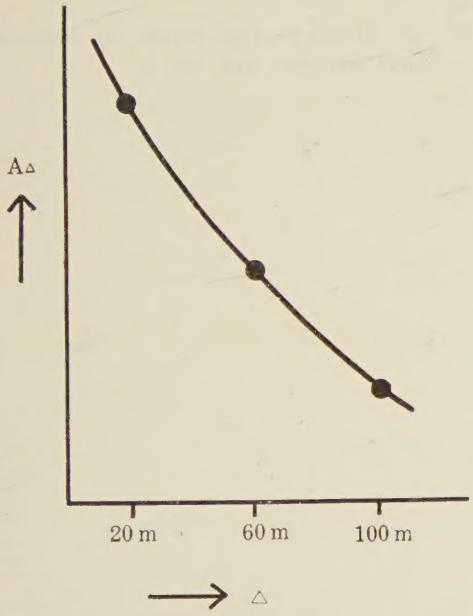

Fig. 11. Effect of shot-receiver distance upon the vertical component of the amlitude of STONELEY waves.

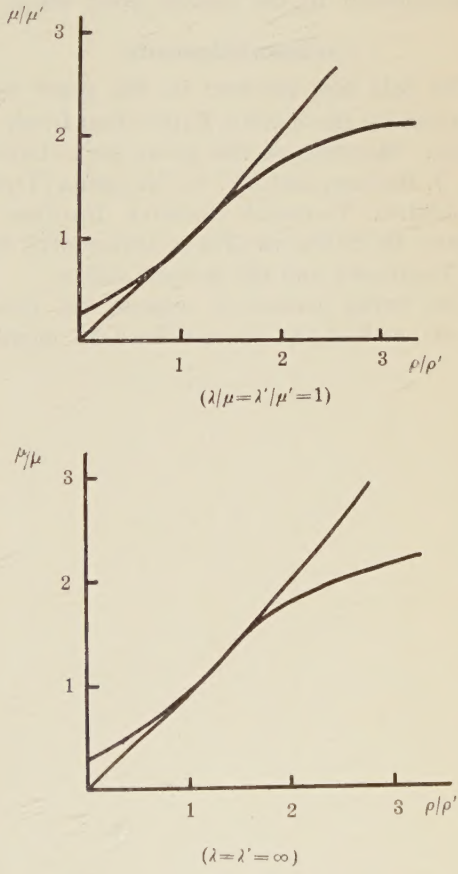

Fig. 12. The range of existence of STONELEY waves. (after K. SEZAWA & K. KANAI and F. G. SCHOLTE.)

boundary wave. In the present experiment, the origin is of dilatational type, because, in general, dynamite explosions initially generate spherical dilatational waves.

The propagation velocity of the observed STONELEY wave was measured as 430 m/sec. The propagation velocity of the STONELEY wave is shown to be nearly equal to that of the transversal wave in the same solid. In the present experiments, the transversal wave velocity was not obtained, but assuming POISSON's ratio of about 0.45, we get the tranversal wave velocity of 430 m/sec. This value of 0.45 is not so unnatural for clay or sand fields.

Unfortunately, the attenuation formula for the STONELEY wave could not be determined experimentaly by the reasons given above.

Acknowledgments

The field data reported in this paper were obtained by the Seismic Exploration Group of Japan. Members of this group are as follows Mr. S. HAYASHI and Mr. N. MIYAZIMA (Transportatation Technical Research Institute of Japan), Dr. S. OMOTE (Tokyo University), Mr. T. YOSHIZAWA and the present author.

The writer wishes to express his hearty thanks to Prof. K. SASSA (The head member of this group), Prof. E. NISHIMURA and Dr. K. KANAI for their many valuable discussions. Many thanks are also due to Mr. H. HAYASHI and Mr. MIYAZIMA for their assistance in these experiments.

References

R. STONELEY
1924. Elastic Waves at the Surface of Separation of Two Solids. Proc. Roy. Soc. London. vol. 106.

K. SEZAWA and K. KANAI
1939. The Range of Possible Existence of STONELEY-Waves and Some Related Problems. Bull. Earth. Res. Inst. Vol. 17.
1938 & 1939. The Formation of Boundary Wave at the Surface of a Discontinuity within the Earth's Crust. I, II.
Bull. Earth. Res. Inst. vol. 16, vol. 17.

F. G. SCHOLTE
1947. The Range of Existence of RAYLEIGH and STONELEY Waves.
M.N.R.A.S.G.S. vol. 5.

T. KAMETANI
1954. Surface Structuies and Surface Layer Corrections. (in Japanese) Report of Seismic Exploration Group of Japan. No. 2.

Y. SATO
1953. On Elastic Surface Waves (in Japanese) Jour. Seis. Soc. Jap. vol. 6.